BLUE AND UV SEMICONDUCTOR LASERS*

S. Krukowski, C. Skierbiszewski, P. Perlin, M. Leszczynski, M. Bockowski, S. Porowski

Institute of High Pressure Physics, Polish Academy of Sciences
Sokołowska 29/37, 01-142 Warsaw, Poland

(Received March 28, 2006)

Despite many technological difficulties the group III nitrides: GaN, AlN and InN and their alloys are primary candidates for electro-optical coherent light sources. In the recent years the research and technology of the nitride based continuous wave (CW) laser diodes (LDs) led to creation of blue-violet coherent light sources of power up to 200 mW. The progress has been attained by using various ways to attack the main obstacles in the technology of these devices such as insufficient size of high quality lattice matched substrates, low *p*-doping efficiency of Mg acceptor, poor contact to *p*-type semiconductor and low efficiency of radiative recombination. The two different approaches were used to overcome the substrate problem: hetero-epitaxy and homoepitaxy. Homoepitaxy used high pressure GaN high quality crystals. Heteroepitaxy used sapphire, SiC or GaAs substrates and very sophisticated techniques of reduction of the dislocation density. The low *p*-doping efficiency by using Mg acceptor is related to creation of Mg–H complexes due to hydrogen presence during the growth of laser diode quantum structures. In addition, Mg acceptor has low efficiency due to its high energy. High Mg concentrations can be obtained by using either MOCVD or ammonia source MBE growth. An alternative route is to use hydrogen-free plasma activated MBE (PA-MBE) method. The recent advances and the prospects of both approaches will be discussed. Solid AlGaInN solution offers a possibility to cover wide spectral range, starting from near UV to blue, green and red. Arsenide based laser diodes (LDs) are efficient coherent red light sources. Therefore, nitride based LDs are considered to be devices of choice for green, blue and UV spectral range. So far only blue and violet laser has been realized. The progress toward green and UV lasers is far less spectacular. The results in all these areas and future prospects will be discussed.

PACS numbers: 81.05.Ea, 68.55.Ac, 81.15.–z, 42.55.Px

* Presented at the PLC2005 Workshop, 5–8 September 2005, Kazimierz, Poland.

1. Introduction

GaN, AlN and InN and their solid solutions became the materials of choice for short-wavelength optoelectronics only recently [1]. These compounds were selected not only due to their wide direct energy gaps, covering the whole visible spectrum and near UV range, but also due to their excellent physical properties such as hardness, physical and chemical stability. Therefore, these materials become a prime object of interest of engineers designing optoelectronic devices that have high energy density in the active regions of the devices.

GaN was first synthesized in the early thirties [2], but its application in electronics was hampered by extreme difficulties of growing it in single crystalline form. The latter fact arises from the thermodynamic properties of GaN which has very high melting temperature — 2220°C that is accompanied by high equilibrium nitrogen pressure close to 60 000 bar [3]. At present the large size substrate quality GaN crystals are obtained by High Nitrogen Pressure Solution Growth (HNPSG) method [4,5]. The size of the crystal reach 2 cm and their thickness is about 100 μm, which allows the manufacturing of high power Laser Diodes (LDs). The production output is sufficient for covering professional application of high power devices on the international scale.

This option is a solution for high power professional devices. Another route to large scale manufacturing of blue laser diodes was proposed [6–9] for mass production. The two different methods are based on application of foreign substrates, such as sapphire, SiC or GaAs. In the first method, called epitaxial lateral overgrowth (ELOG), GaN template layers are deposited in the standard way, by MOVPE or HVPE method, on the surface of high quality substrate. Then an important step is deposition of the mask, usually SiO_2 [6,8] or TiN [7] which covers the most of the surface. Subsequent growth of GaN allows to obtain thick GaN substrate with the dislocation density of about 10^7 cm^{-2}.

The alternative method, called hetero-epitaxial lateral overgrowth (HELO) relies on the deposition of the mask directly on the foreign substrate [9]. The process omits the template growth. The thick GaN layer is then deposited directly on the substrate. The early stage of the growth is characterized by the independent growth of GaN islands. Afterwards the GaN islands coalesce and the mirror-like GaN surface is developed.

Depending on the growth method, the GaN layer can be either removed from the substrate or it can be used directly to growth of laser quantum structures. The removed GaN layer creates so called free-standing GaN substrate which can be used for the deposition of laser structures. The process is

difficult to control, but it provides large area (two inch) GaN wafers. These wafers have at present about dislocation density of 10^6–10^7 cm^{-2}, which is sufficient as substrates for the manufacturing of small number of relatively high power blue LDs [6–9]. However, the issue whether this method can be used for mass production of low power blue LDs remains to be solved. Similarly the more difficult problem of high quality substrates for high power blue, green and UV LDs is open.

The HVPE growth of GaN on sapphire substrate was used already in 60-ties to obtain first high quality GaN layers, which were used to determine the physical properties of gallium nitride [10–13]. It was established that GaN layers have high concentration of electrons. The attempts to dope for p-type were not successful, which was the largest obstacle to highly efficient optoelectronic devices. The results of doping were so disappointing that large scale efforts to obtain GaN based light emitting diodes (LEDs) were abandoned in 70-ties.

The comeback of nitrides occurred in 1989 thanks to Japanese scientists Amano and Akasaki who discovered the method of activation of Mg acceptors by electron irradiation and obtained first p-type GaN layers [14]. Later Nakamura discovered an industrially important method of activation of Mg acceptors by annealing in hydrogen-free atmosphere [15]. Nakamura improved considerably MOVPE technique to grow nitride (GaN, InGaN) layers on sapphire substrates by introducing low temperature nitride (AlN or GaN) buffer layers and annealing before the second growth stage. From this time on the technology of mass production of high brightness blue and green light emitting diodes (LEDs) was developed with the use of sapphire substrates [1].

It has to be noted, that the technology for laser diodes is far more demanding with respect to crystallographic quality of the substrates and the deposited layers. Despite great technical difficulties, Nakamura obtained the first blue LD in 1996 [16]. The result was obtained by considerable improvement of the crystallographic quality of the MOVPE grown nitride layers using epitaxial lateral overgrowth (ELOG) technique [1]. Since then, the progress in this technology led to the creation of the blue laser which was commercialized. At present 50 mW continuous wave (CW) blue lasers are offered to the market. The progress has been, however, much slower than expected [17] and the mass production of blue laser diodes has not yet been achieved.

The progress in the related segments of green and UV devices is even slower. Superbright green LEDs were also developed by Nakamura and offered to the market as soon as the blue ones. In contrast to that, green LDs have not been obtained. The poor result in the green laser challenge is related to the difficulty in growing high quality In-rich structures by the

MOVPE technique [28]. This involves serious technical difficulties and the green nitride based laser has not been created so far.

The progress in the technology of UV devices has been even slower. It was related to the poor efficiency of quantum well structures grown without indium. It has to be noted that the role of indium, dramatically increasing light emission efficiency, has not been elucidated. The AlGaN structures typically used for UV emitters are less effective emitters. Therefore, both UV LEDs and LDs are far behind their blue/violet counterparts.

An important aspect of the technology of all nitride based devices is p-type doping. Magnesium is still the only effective acceptor. Relatively high ionization energy (200 meV in case of GaN) limits the fraction of ionized acceptors to 1% at room temperature. This problem is aggravated by low mobility of holes in nitride layers. Together it deteriorates electrical properties of GaN and AlGaN layers and electric contact to p-type. This causes intensive heat generation, which is a serious problem for high power devices.

Despite these problems, the heteroepitaxial nitride technologies progressed fast and at present the highly efficient blue LEDs are produced at relatively low cost. The later stage directed to laser technology has been less successful. As the result, low cost blue/violet LDs were not marketed. This has created a new chance to homoepitaxial technology. The homoepitaxy was developing slowly at early stage because of the difficulties in obtaining large, high quality GaN crystals which could be used as substrates for epitaxial deposition of multilayer quantum structures necessary for devices. This is a direct consequence of thermodynamic properties of GaN [5] (and also AlN [19]), in particular, its melting conditions which are so extreme, that the application of the common growth methods from stoichiometric liquids is technically impossible. The most successful method of growing the dislocation-free GaN crystals so far is the growth of GaN under high pressure of nitrogen.

High pressure (HP) grown low dislocation density GaN crystals were used as substrates for MOVPE and MBE epitaxial deposition. The standard blue/violet laser diodes obtained by these methods in the Institute of High Pressure Physics of PAS (IHPP PAS) have the comparable parameters. The Plasma Assisted Molecular Beam Epitaxy (PA-MBE) technique offers unique possibility to grow laser structures in hydrogen-free atmosphere. Also the new structures for green and UV LEDs were successfully grown. It is expected that in the near future, both green and UV laser diodes could be developed by using PA-MBE technique. The results and the prospects for the near future will be described in this paper.

2. High pressure crystallization of GaN

2.1. Thermodynamic properties of GaN-Ga-N_2 system

The thermodynamic properties of group III nitrides: AlN, GaN and InN cause great difficulties for the direct growth of high quality bulk crystals of these compounds. Similar to diamond, the growth of high quality single GaN crystals requires the use of very high pressures. As shown in Table I, AlN, GaN and InN melting temperatures and pressures far exceed those of the typical semiconductor materials. The melting temperature TM, and the corresponding equilibrium pressure at melting, of GaN, AlN and InN are very high and the experimental determination of the melting point is extremely difficult. For AlN and InN these coordinates has not been measured [19]. The quoted melting temperatures have been calculated by the use of Van Vechten's Quantum Dielectric Theory of Chemical Bonding [20]. The corresponding pressure follows from the extrapolation of the experimental equilibrium data [21, 22]. Utsumi *et al.* reported congruent melting of GaN at 2220°C at pressure about 60 kbar [3]. Table I shows that both the temperature and pressure at melting of GaN are much higher than that for typical semiconductors. They are rather similar to the conditions used for high pressure synthesis of diamond [23] or peritectic point for SiC [24].

TABLE I

Melting conditions of selected semiconductors.

crystal	T^{M}, K	p^{M}, bar
Si	1685	< 1
GaAs	1510	15
GaP	1750	30
AlN (estimated [19])	3500	200
GaN — [3]	**2490**	**60 000**
InN(estimated [25, 26])	2200	>60 000
SiC(sphalerite-peritectic point [24])	3100	>100 000
C(diamond-estimated [23])	5000	150 000–300 000
Diamond (synthesis)	1600	60 000

Due to these extreme melting conditions, GaN (like AlN [19] and InN [26]) cannot be grown from its stoichiometric melt by the Czochralski [27] or Bridgman [28] methods commonly used for typical semiconductors. It has to be crystallized by methods which allow to grow the bulk crystals using lower temperatures and pressures.

Gallium nitride is a strongly bonded compound (with bonding energy of 9.12 eV/atom pair [29]) in comparison with typical III-V semiconductors

like GaAs (bonding energy of 6.5 eV/atom pair [29]). Consequently, the free energy of the crystal is very low in relation to the reference state of free N and Ga atoms. On the other hand, the N_2 molecule is also strongly bonded (4.9 eV/atom). Therefore, the free energy of GaN constituents at their normal states, Ga and N_2, becomes quite close to that of the crystal. It is illustrated in Fig. 1 where the free energy of GaN (1 mole) and the free energy of the system of its constituents (Ga + $1/2N_2$) is shown as a function of temperature and N_2 pressure.

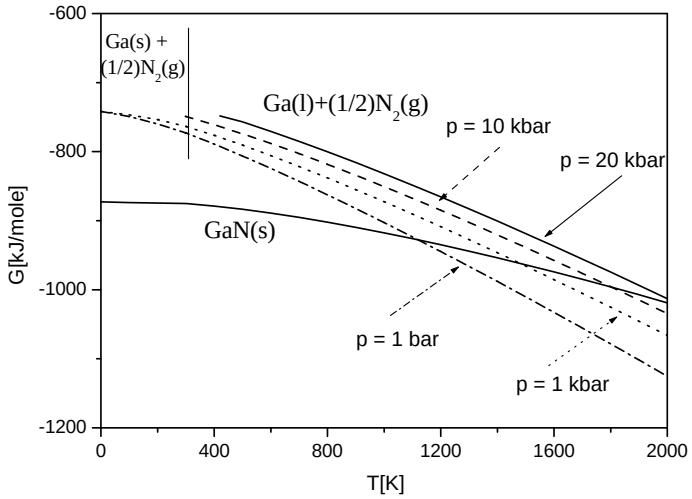


Fig. 1. Gibbs free energy of GaN and its constituents as a function of the temperature: Ga + N_2 GaN — thick solid line, the constituents: Ga + N_2 — $p = 1$ bar dash-dotted line, $p = 1$ kbar — dotted line, $p = 10$ kbar — dashed line, $p = 20$ kbar — solid line.

With increasing temperature, Gibbs composite free energy of the constituents $G_{\mathrm{Ga}+1/2\mathrm{N}_2}(T)$ decreases faster than $G_{\mathrm{GaN}}(T)$ of the crystal and at higher temperatures, the nitride becomes thermodynamically unstable. The crossing of $G(T)$ curves determines the equilibrium temperature at which GaN coexists with its constituents at given N_2 pressure. The application of pressure increases the free energy of the constituents in much higher degree than $G(T)$ of the crystal. As a consequence the equilibrium point shifts to higher temperatures and GaN stability range is extended.

The equilibrium p_{N_2}–T conditions for GaN were studied by several groups. The most complete and consistent results were obtained by Karpinski *et al.* [21, 22] by direct synthesis and decomposition experiments performed by both gas pressure technique (for pressures up to 20 kbar) and high pressure anvil technique (up to 70 kbar). The curve following from these data is shown in figure 2.

Crystallization processes discussed in this paper have been carried-out at N_2 pressure up to 20 kbar which corresponds to GaN stability limit of 1960 K. These conditions are marked in Fig. 2. As it was shown in Ref. [22] for pressures up to 20 kbar, the equilibrium curve can be described by the van't Hoff equation

$$\Delta H_{\mathrm{F}} = \frac{1}{2} R \frac{d \ln a_{\mathrm{N}_2}}{d(1/T)}\,, \tag{1}$$

where ΔH_{F} is the formation enthalpy of GaN, $a\mathrm{N}_2$ is the equilibrium activity of N_2 gas, with ΔH_{F} constant and equal to -37.7 kcal/mole. The extension of GaN stability range by the application of pressure allows growing GaN crystals from the solution in the liquid Ga. In Fig. 3 we show the experimental N solubility data [29].

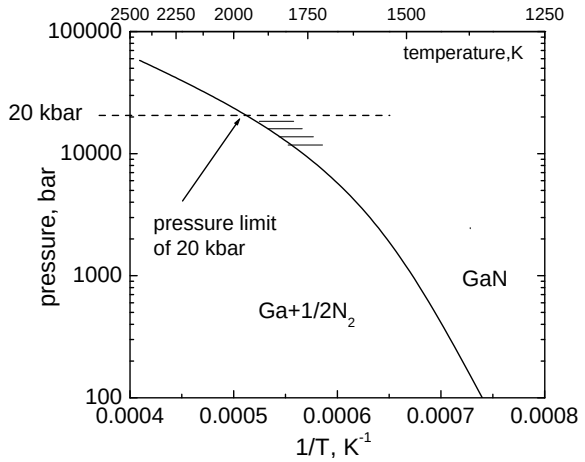


Fig. 2. p–T phase diagram of GaN(s)–Ga(l)–N2(g) system, determined by Karpinski *et al.* [21, 22]. The shaded area corresponds to HNPSG of GaN.

Even the highest experimentally accessible temperature 1960 K is considerably below the melting temperature of GaN (Table I). Therefore the N concentrations are not high (below 1 at.%) at the accessible growth temperatures and the growth experiments have to last long to obtain high quality crystals with dimensions appropriate for application as substrates for epitaxy. Therefore, the long time (over 200 h) of stable work is necessary. The solid line in Fig. 3 is the liquidus line for Ga–GaN system calculated in ideal solution approximation with Van Vechten's melting temperature of 2790 K [20]. For this approximation the solubility can be expressed as follows:

$$n = n_0 \exp \frac{\Delta H_{\mathrm{sol}}}{kT}\,, \tag{2}$$

where ΔH_{sol} is the heat of dissolution. Using the approximation to the experimental solubility data for GaN, the following heat of dissolution was obtained: $\Delta H_{\mathrm{sol}} = 44.7$ kcal/mole $= 0.49$ eV/bond. The heat of dissolution expresses the difference in bonding energies in the crystal and its mother phase — the solution [29].

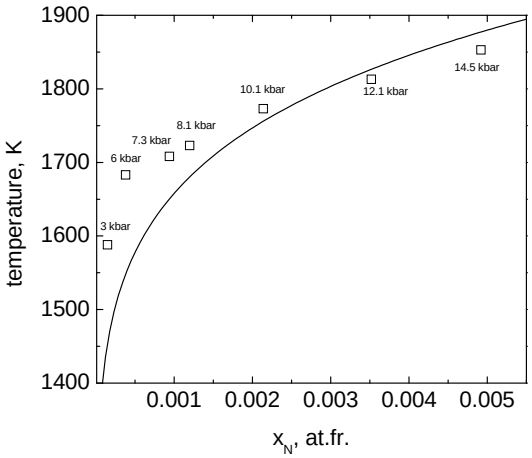


Fig. 3. Nitrogen solubility in liquid Ga: points — experimental data [29], line — ideal solution approximation calculated using the Van Vechten estimate of GaN melting temperature [20].

The analysis of thermodynamic properties of the system of GaN and its constituents explains the role of high pressure as a factor increasing thermodynamic potential of the constituents (mainly nitrogen) which allows the GaN crystal to be stable at temperatures necessary for effective crystallization. The pressure, however, is important also for kinetics of GaN synthesis. It is analyzed in the next section.

2.2. Dissolution kinetics and its influence on crystal growth

The kinetic properties of GaN–Ga(l)–N_2 such as high energy barriers considerably affect the GaN crystallization, limiting the possible growth to high temperature and, consequently, high nitrogen pressures. As we will see, the kinetic properties are also much different from other III-V systems which entails the use of specific experimental crystal growth techniques. This also affects the models used in the description of the microscopic properties of the system and numerical simulation procedures.

Though physical properties of these three involved phases are distinctly different, ranging from the gas (N_2) to metallic liquid (Ga) and semiconductor solid (GaN), they have some common features. The most important is

that the atoms in all three phases are extremely strongly bonded. Molecular nitrogen is the strongest bonded diatomic molecule in nature, the dissociation energy of N_2 molecule is 9.76 eV [29]. Gallium liquid is characterized by high enthalpy of evaporation 271 kJ/mole (2.81 eV/atom) which is reflected by the critical temperature, close to 4000 K [30, 31]. Similarly, solid GaN is strongly bonded, with the energy 9.12 eV/atom pair, which leads to high melting temperature, close to 2500 K [3].

GaN synthesis from its constituents proceeds via dissolution of nitrogen in liquid gallium, transport of nitrogen to the cold part of the liquid and the growth from the solution. These stages include dissociation of the N_2 molecule which ought to be characterized by high energy barrier. It is expected that the dissociation process involve significant change of the binding energy of the molecule, highly exceeding the typical thermal motion energies which, for the GaN growth conditions, are close to 0.15 eV.

It is likely that the dissociation occurs during the adsorption of the N_2 molecules on liquid Ga surface. This possibility was investigated by solving quantum mechanical many body problem with the use of density functional method (DFT) formulation [32]. Since thermal motion of the Ga atoms plays a minor role, Born–Oppenheimer approximation can be used. An infinite Ga surface can be simulated by a finite cluster of Ga atoms [33, 34].

The two different orientation of N_2 molecule: parallel and perpendicular to the surface were used in the calculations [33]. The obtained results include the electron charge distribution, the position of the atoms, and the total

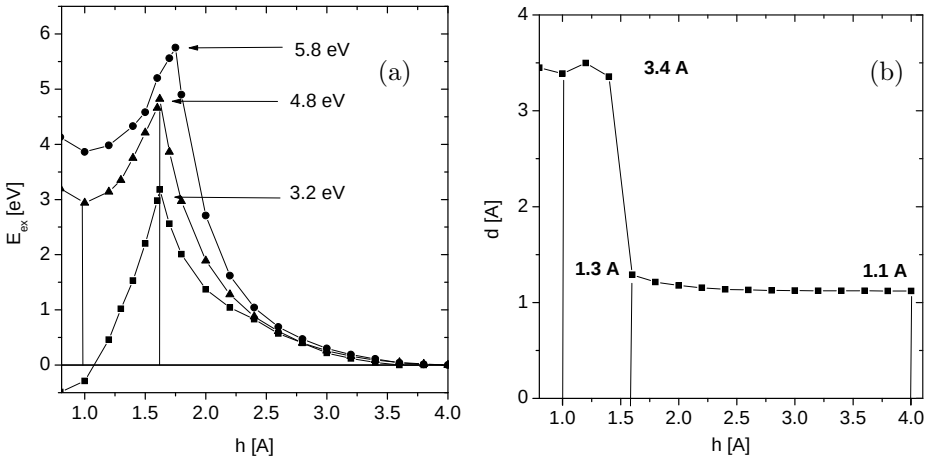


Fig. 4. (a) — Excess energy of the system as a function of the distance between the N_2 molecule and metal cluster: squares — Al, triangles — Ga, circles — In. (b) N–N interatomic distance as a function of the distance between the N_2 molecule and Ga cluster.

energies of the system. In Fig. 4(a) we present the change of the total energy of the system as a function of the distance between the Ga surface and the N_2 molecule. In these data the parallel orientation of the molecule to the surface has been used. The interaction is negligible for distances higher than 4 Å for which the excess energy zero level is adopted. For closer distances the energy increases sharply to reach 4.8 eV for $d = 1.6$ Å and then sharply decreases. As shown in Fig. 4(b), the excess energy increase occurs when the N–N distance is only slightly increased whereas the decrease occurs after the N–N distance increased suddenly to more than 3.2 Å. This dramatic change indicates that at the distance 1.6 Å, the dissociation of the N_2 molecule takes place.

The dissociation of the N_2 molecule into separate N atoms is confirmed by the plot of the electronic charge distribution, presented in Fig. 5. The surface corresponding to selected density the electron charge was plotted for the three following Ga–N_2 distances: 4.0 Å, 1.6 Å and 1.0 Å. These distances are denoted in Fig. 4(a) and (b) by vertical dashed lines. For the first two cases the electronic charge is concentrated in the region between N atoms, for the last case the charge is shifted to the region between Ga and N atoms, confirming dissociation of N_2 molecule and creation of chemical bond between two N atoms and Ga surface atoms.

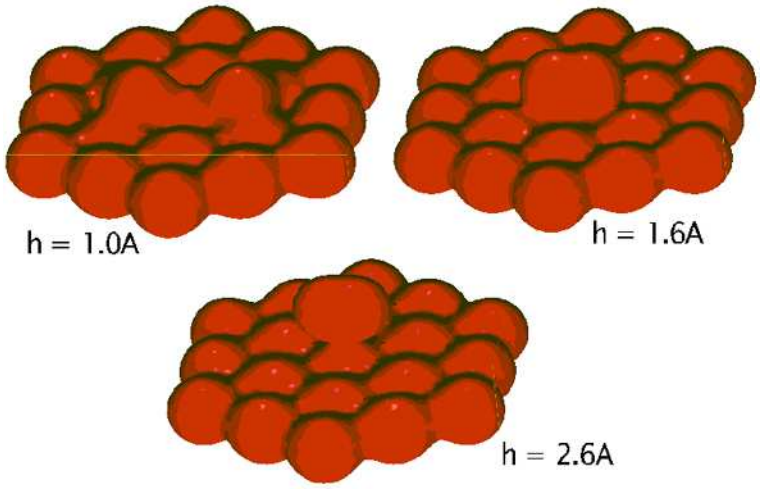


Fig. 5. Electronic charge constant density surface for N_2, parallel to 19 atoms Ga cluster for three selected N–Ga distances: $h = 2.6$ Å, $h = 1.6$ Å and $h = 1.0$ Å.

Similar change of the total energy and N–N interatomic distance is obtained for surfaces of other group III metals: Al and In. The dissociation energy barriers are the following: 3.2 eV for Al and 5.8 eV for In, all much

lower than the N_2 dissociation energy, which indicates strong catalytic influence of group III metal surface.

The calculation of the interaction of the N_2 molecule, oriented perpendicular to Ga surface also confirmed the dissociation of the molecule. Generally, the energy barriers are much lower for this orientation: 3.0 eV for Al, 3.4 eV for Ga and 3.6 eV for In. Since the interatomic distances are much larger for a In cluster, one can expect that the energy barrier for Al and Ga are relatively overestimated due to larger stiffness of these two clusters.

The nitrogen dissociation rate on the metal surfaces was calculated by using these energy barriers. In these calculations the vibrational energy was accounted for. Since the energy barrier is much higher for the parallel than for perpendicular N_2 orientation, the rotational energy was neglected. The impingement rate was obtained from the ideal gas approximation. The reaction rate was determined as the fraction of the molecule which can penetrate over the energy barrier determined from the QM calculations and is given by the following formula:

$$R = \frac{p}{\sqrt{2\pi\, mkT}} \left[1 + \frac{E_{\mathrm{bar}}}{kT}\right] \exp\left(-\frac{E_{\mathrm{bar}}}{kT}\right), \tag{3}$$

where the second term in the square bracket stems from the contribution of the vibrational energy. Using this formula the dissociation rate can be

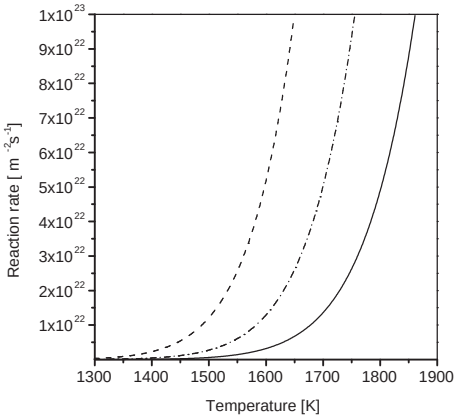


Fig. 6. Average dissociation rate of N_2 on liquid group III metal surface calculated using ideal gas approximation; Al — dashed line; Ga — dash-dotted line; In — solid line.

calculated for given temperature and pressure of the nitrogen. The temperature dependence of the nitrogen dissociation reaction rate for Ga, Al and surfaces, for the gas pressure 20 kbar is presented in Fig. 6.

The nitrogen dissolved in the hot end Ga surface is transported into the cold part of the liquid by convection and diffusion. There the GaN growth proceeds via three main stages. The initial stage is a heterogeneous nucleation of GaN on the Ga surface. During the second stage the growth of numerous GaN crystals and separation of the dominant growth centers occurs. And the final stage is the growth of small number of single crystals in the supersaturated solution of N in liquid Ga. The last stage determines the results of the crystallization process.

2.3. Crystal growth of GaN by high nitrogen pressure solution (HNPSG) method — experimental

The Institute of High Pressure Physics has developed the technology of crystallization at high nitrogen pressure. This includes the technology of large volume high pressure vessels [35], internal heating furnaces, the properties of material at high pressure and temperature [36], pressure and temperature control and stabilization techniques [5]. At present, GaN is crystallized in gas pressure chambers with volume up to 5000 cm^3 which allow the use of the crucibles with the working volume of 50–100 cm^3. The high pressure–high temperature reactor consisting of the pressure chamber and the multizone furnace is equipped with additional systems necessary for *in situ* annealing in vacuum, electronic stabilization and programming of pressure and temperature, and cooling of the pressure chamber. The pressure in the chamber is stabilized with the precision better than 10 bar. The temperature is measured by a set of thermocouples arranged along the furnace and coupled with the standard input power control electronic systems based on Eurotherm units. This allows stabilization of temperature of ± 0.2 K and programmable changes of temperature distribution in the crucible. The example of high pressure apparatus, constructed in HPRC, is presented in figure 7.

The GaN crystals presented in this paper were grown from the solutions in pure liquid gallium and in Ga alloyed with 0.2–0.5 at.% of Mg or Be at pressures in the range of 10–20 kbar and temperatures of 1700–2000 K. Magnesium and Beryllium as the most efficient acceptors in GaN were added to the growth solutions in order to reduce the concentration of free electrons in the crystals by compensation of residual donors.

The supersaturation in the growth solution has been created by the application of temperature gradient of 2–20 K/cm along the axis of the crucible. This method was chosen since the axial temperature gradients in multi-zone



Fig. 7. High pressure crystal growth apparatus, constructed in the Institute of High Pressure Physics for crystallization of GaN. The maximum working nitrogen pressure is 15 kbar, the maximum temperature — 1600°C, the internal diameter — 100 mm.

furnaces working at high gas pressure can be controlled with high precision and the method assures a continuous flow of nitrogen from the hotter part of the solution to the cooler one. Since the crystallization growth processes were performed without an intentional seeding, the crystals nucleated spontaneously on the internal surface of polycrystalline GaN crust, covering liquid Ga at the cooler zone of the solution. Typical duration of the processes was 120–200 hours.

The slow cooling at isothermal conditions was not applied due to small concentrations of nitrogen in the liquid gallium (Fig. 3). The crystallization at constant temperature, at N_2 overpressure was not applied as well since then the crystallization can occur only on the Ga surface and stops if the whole surface covers with GaN.

2.4. GaN single crystals

2.4.1. Crystals grown without intentional seeding

The GaN crystals grown by the High Nitrogen Pressure Solution method are of wurtzite structure, mainly in the form of hexagonal platelets. The structure of GaN crystal is presented in figure 8. As shown in the figure, the subsequent planes consist of the atoms of the same kind. In one these two planes, the atoms are bonded to three atoms. From the upper side these atoms are denoted as black in the lower by yellow. These planes are energetically stable, therefore the sides are denoted as N-side and Ga-side, respectively.

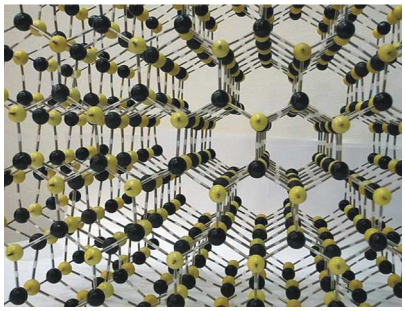


Fig. 8. The crystallographic structure of GaN crystals. Ga and N atoms are denoted by black and grey color, respectively.

The large hexagonal surfaces of bulk GaN crystals correspond to {0001} polar crystallographic planes. Conventionally the N-side is denoted as {000−1} and Ga-side as {0001} surface. The side faces of the crystals are mainly the polar {10−11} and also non-polar {10−10} planes.

The crystals in the form of hexagonal platelets grown slowly, with a rate below 0.1 mm/h along [10$\underline{1}$0] direction (perpendicular to the *c*-axis), are usually single crystals of perfect morphology suggesting stable layer-by layer growth. They are transparent, with flat mirror-like faces. The habit of the crystals does not change for solutions containing Mg or Be.

As one can deduce from the form of the crystals the growth is strongly anisotropic, being much faster (about 100 times) in directions perpendicular to the *c*-axis [37]. This relation is valid at supersaturations corresponding

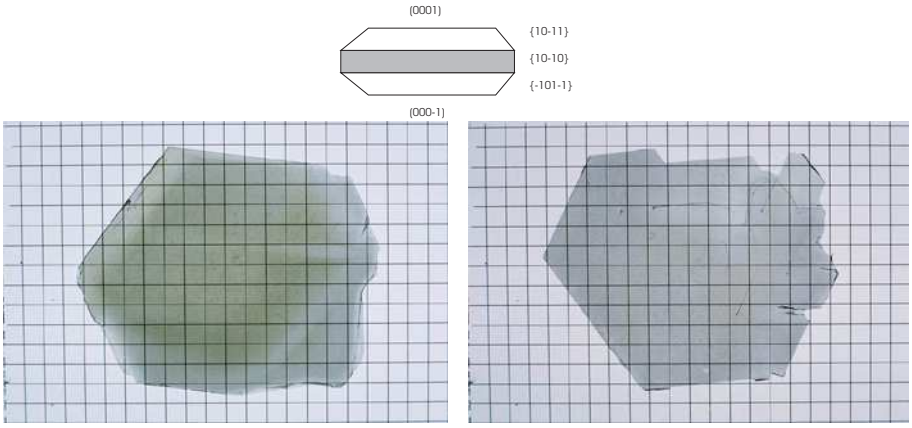


Fig. 9. GaN crystals grown using high nitrogen pressure. The distances between grid lines correspond to 1 mm. The schematic cross-section of the hexagonal platelet is shown in the upper part.

to the average growth rate in $\{10{-}10\}$ directions of 0.05–0.1 mm/h. As will be shown in the next section, the domination of the growth in the plane perpendicular to the c-axis is typical to relatively low supersaturations.

As it is shown in the next section, high supersaturations enhance the growth into c-direction which, unfortunately, leads to the unstable needle-like forms. The supersaturation in the growth solution is determined mainly by the growth temperature, temperature gradients, mass transport mechanisms in gallium and also by the local surrounding for a particular crystal (*i.e.* the presence of neighboring crystals). For crystallization of large GaN crystals, it is crucial to control the supersaturation in order to avoid acceleration of the growth near edges and corners of the growing crystal. If supersaturation is too high, the edge nucleation on hexagonal faces of GaN platelets is often observed, which is the first step to the unstable growth on that faces.

The polarity of the crystal surfaces was identified by etching in hot alkali water solutions since the Ga-polar surface is inert to etching whereas the N-polar one etches well for both types of crystals. The method was calibrated by CBED [38, 39] and XPS [40] measurements.

2.4.2. Crystals grown without intentional seeding — 2-d nucleation controlled growth rate

Due to high bonding energy and crystallographic structure of main surfaces, the growth of GaN crystals is strongly anisotropic. This is reflected in the shape of GaN crystals which is hexagonal platelet or hexagonal needle.

It follows from that observation that for the case of plate-like crystals, the growth rates are the fastest for $\{10\underline{1}1\}$ and $\{10\underline{1}\bar{1}\}$, slower for $\{10\underline{1}0\}$ and the slowest for $\{000\underline{1}\}$ and $\{000\underline{\bar{1}}\}$ surfaces. In case of the needle-like crystals the velocity ordering is reversed. For both cases the flat faces of GaN crystals indicate that they grow by 2-d or layer-by-layer mechanism.

One of the most efficient growth centers are screw dislocations. Since in the GaN wurtzite structure screw dislocations have much higher energies than edge dislocation, their fraction in total dislocation density is small. In case of the growth of good quality GaN crystals, the role of screw dislocation is negligible.

In absence of the screw dislocation the morphological properties of GaN growth results from the competition between the nucleation and completion of new layers. These two processes have different size dependence. At stable thermodynamic conditions at the surface the nucleation rate is proportional to the surface whereas the completion rate is inversely proportional to the dominant linear size of the surface. In most cases it is proportional to the inverse of the square root of the surface. Hence one can expect that, for some cases, the transition from the nucleation to completion controlled growth occurs.

Growth controlled by 2-d nucleation is morphologically stable. In most cases the surfaces $\{10\bar{1}0\}$ and $\{000\bar{1}\}$ are atomically flat with several steps. The growth rate can be assessed using Becker–Doring nucleation law [41]. The rate is strongly dependent on supersaturation at the surface. Assuming that the edge energy is due to 2 broken bonds per atom site and using dissolution energy as the broken bond energy difference, the rate can be expressed as a function of the supersaturation [23]. For experimental growth rates, these calculations give 48% supersaturation at the growth zone, which is in good agreement with the estimation obtained from the temperature difference in the crucible and the x–T phase diagram [23].

In case of the other GaN faces the surface is not so flat. This is typical for the growth controlled by step flow where nucleation rate is so fast that it allows to obtain numerous 2-d nuclei at various parts of the surface before the layer is completed. This can be caused either by the step pinning due to the kink poisoning by the impurities or by extremely fast nucleation resulting from relatively high supersaturation. Also the presence of screw dislocation growth centers can cause similar effect. The resulting growth is much faster in some part of the surface leading to the creation of hill and valley morphology and the transition to the morphologically unstable forms. This type of the growth is observed sometimes in the growth on $\{0001\}$ surfaces.

The relative rates on the various faces of GaN crystals can be estimated by using 2-d nucleation controlled growth. In the following we assume that

the change of supersaturation on the face is negligible. This is a good approximation due to relatively small size of the crystal and very low growth rates. Therefore, the diffusion in the liquid homogenizes the concentration relatively fast and the growth proceeds in the uniform, stationary concentration.

The 2-d growth rate can be expressed by using Becker–Doring nucleation formula [41]. The nucleation rate is treated as thermally activated process with the energy barrier calculated as the difference of the volume and surface terms. The total rate for unit of the surface area I is expressed as the average frequency of attaching a molecule ν at the nucleus circumference and the probability of overcoming the energy barrier ΔG^*:

$$I = x_s q \nu \exp\left(-\frac{\Delta G^*}{kT}\right), \tag{4}$$

where x_s is the concentration of the nitrogen in the solution at the GaN surface, q is the number of the sites at the circumference of the 2-d nucleus.

Due to the different atomic structure of the different faces both the number of sites at the circumference and the energy barrier are different for the various faces of GaN crystal. For the (0001) face the lowest surface energy is for the hexagonal shape of the nucleus, whereas for (10−10) face the square is the most favorable one [37]. These shapes are presented in Fig. 10.

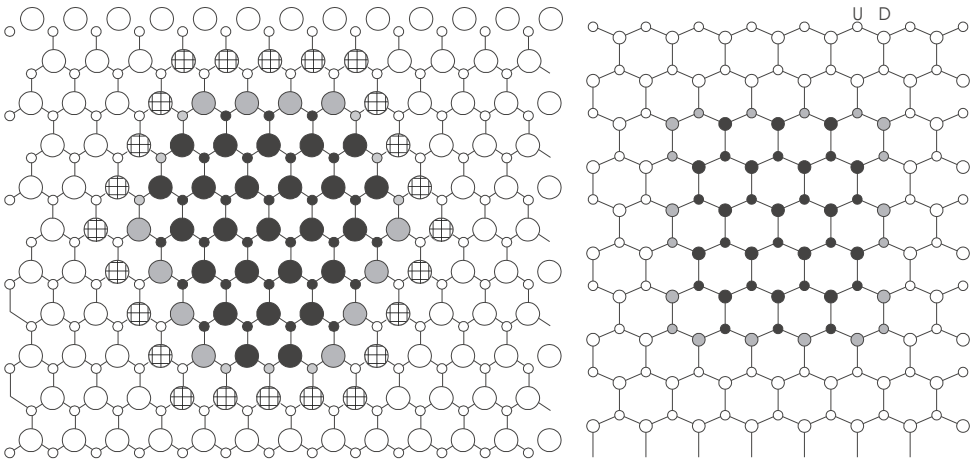


Fig. 10. 2D — nuclei on the (0001) and (10−10) surfaces of GaN, (a) and (b), respectively. Grey atoms belong to the edges of the nuclei.

Using this formulation the 2-d nucleation rates can be expressed as the difference between the equilibrium and actual chemical potentials function $\Delta\mu$ which can be expressed in terms of the supersaturation σ and the temperature T:

$$\Delta\mu = RT \ln \sigma = RT \ln \left(\frac{x - x_{\mathrm{eq}}(T)}{x_{\mathrm{eq}}(T)} \right), \tag{5}$$

where x and $x_s(T)$ are the nitrogen concentration at the GaN surface and the equilibrium concentration at the growth temperature (Fig. 3).

For the polar (0001) surface, the nucleation rate is [37]:

$$I = \nu x_s \left(\frac{6\phi}{\Delta\mu} + 6 \right) \exp \left[-\frac{1}{RT} \left(\frac{3\phi^2}{\Delta\mu} - \frac{3\Delta\mu}{4} \right) \right], \tag{6a}$$

whereas for the (10−10), the nucleation rate is [37]:

$$I = \nu x_s \left(\frac{4\phi}{\Delta\mu} - 1 \right) \exp \left[-\frac{1}{RT} \left(\frac{2\phi^2}{\Delta\mu} - \frac{\Delta\mu}{8} \right) \right], \tag{6b}$$

where ϕ is the bond energy, estimated from the GaN heat of the dissolution. The 2-d nucleation rates in function of the supersaturation σ are graphically presented in Fig. 11 below.

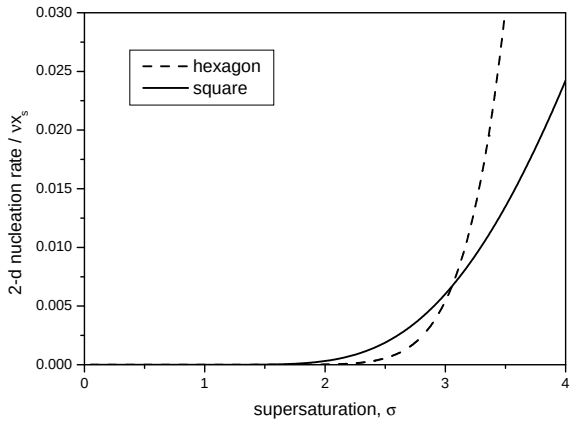


Fig. 11. Relative 2D-nucleation rates on the (0001) and (10−10) surfaces of GaN estimated with the use of heat of dissolution following from the experimental solubility data.

The above dependence qualitatively recovers observed experimental change from the plate-like growth habit for low to needle-like for the high supersaturations [29]. In order to obtain the quantitative agreement the most advanced calculations, based on *ab initio* quantum DFT approach, are necessary.

2.5. Physical properties of GaN grown by HNPS method

2.5.1. Point defects

As it was already mentioned, the N_2 molecules dissociate at the contact with the Ga surface. However, to approach the surface they have to overcome quite high (about 3.5 eV) potential barrier which lowers substantially the rate of nitrogen dissociation and its further dissolution in the metal. For oxygen interacting with Ga, there is no potential barrier for dissociation [42] and therefore even traces of this impurity in the growth system are source of the unintentional oxygen doping of GaN. Consequently the crystals are strongly *n*-type with free electron concentration of about 5×10^{19} cm^{-3} (metallic conductivity) and mobility of about 60 cm^2/Vs [43]. These free carriers can be fully eliminated by a Mg acceptor added into the growth solution. Then the resistivity of the crystals becomes as high as 10^4–10^6 Ωcm at 300 K. Usually the GaN:Mg crystals become *p*-type with the activation energy of 200 meV, at temperatures slightly exceeding 300 K. More detailed analysis of the electrical properties of pressure grown Mg doped GaN crystals can be found in Ref. [44].

The presence of the native point defects in the crystals has been checked by positron annihilation measurements [45]. High concentration of Ga vacancies V_{Ga} has been found in the conductive crystals in contrast to the Mg-doped samples where no Ga-vacancies have been observed. This agreed with theoretical prediction that the formation energy of V_{Ga} decreases with the increase in the Fermi level energy [46,47] suggesting that in the creation of these defects thermodynamics plays a role. The difference in the PL spectra [48] of the conductive (strong yellow emission) and Mg-doped crystals (no yellow emission, blue Mg-related signal) supported the view that V_{Ga} is involved in yellow luminescence in GaN.

Some faces corresponding to the polar low index {0001} and {10−11} crystallographic planes in wurtzite structure, appearing in the pressure grown GaN crystals are non equivalent regarding their atomic structure. This reflects in the asymmetry of the physical properties of the plate like crystals grown without an intentional seeding. In Fig. 12 there is the example of such an asymmetry. The figure shows that the material grown with N-polarity differs in its PL properties from the material grown with the Ga-polarity which indicates that the point defects incorporate into the crystal in different ways. Additionally the spectra coming from the material grown on the {0001} N- or Ga-polar surfaces (seeded growth) are of similar character that the spectra from corresponding surfaces of the substrate. Since the platelets were polished before being used as seeds, the suggestion arises that the platelets themselves also demonstrate a polar character despite they were grown mainly in the fastest growth <10−10> directions what follows from their morphology.

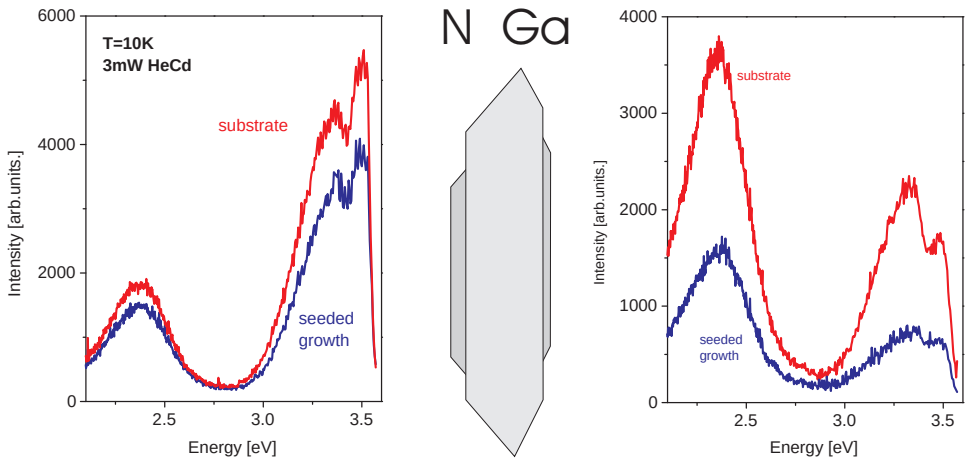


Fig. 12. Photoluminescence of GaN layers grown on different sides of HP grown GaN substrate and the substrate itself. Center — scheme of the layers and the substrate.

The strong support for that are the measurements of the free electron concentration distribution across the cleaved, as grown GaN platelet by the micro Raman scattering technique [49], presented in Fig. 13. The results prove that the difference between materials of higher (N-side) and lower (Ga-side) electron concentration is abrupt. This suggests that the microscopic (in the atomic scale) processes responsible for the formation of both native

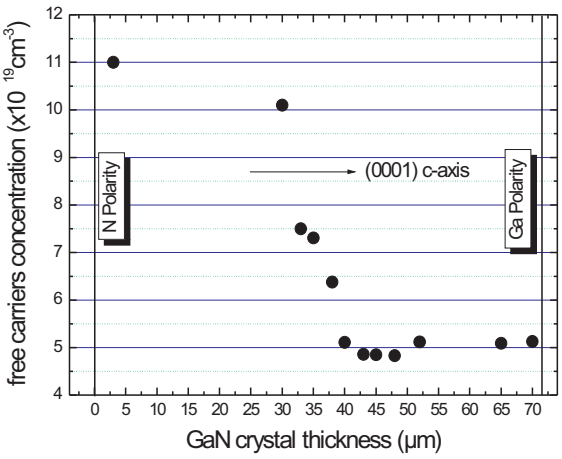


Fig. 13. Distribution of free electron concentration across the GaN platelet measured by micro-Raman scattering technique [41].

and impurity related point defects are related to the kinetic factors related to the growth on different faces of GaN. It also indicates that the diffusion of the donors which are the sources of the free electrons, is negligible at the growth temperature.

Such approach allows to understand yet another result of positron annihilation measurements [50], showing that the concentration of Ga vacancies is much higher at the Ga-side than at the N-side of the n-type GaN platelets. It seems surprising at the first sight, since on the Ga-polar (0001) surface, the surface Ga atoms are bonded to the surface by three bonds whereas to the opposite one only by a one bond. If we assume, however, that the incorporation of the Ga atoms occurs on the $\{10{-}11\}$ polar surfaces, the positron annihilation results become more consistent since on the $(10{-}11)$ face adjacent to the (0001) one, the Ga atoms can be bonded by one or two bonds whereas on the opposite $(-101{-}1)$ polar surface adjacent to the $(000{-}1)$ one, the Ga surface atoms are bonded by two or three bonds.

2.5.2. Extended defects

The structure of the pressure grown GaN crystals has been investigated using various techniques, including X-ray diffraction (XRD) [51], transmission electron microscopy (TEM) *i.e.* [38, 52–54], defect selective etching (DSE) [55] and atomic force microscopy (AFM) of the homoepitaxial layers [56].

In case of the conductive crystals, the shape of the X-ray rocking curves ((0002)CuKα reflection) depends on the size of the crystal. The full widths at half maximum (FWHM) are 20–30 arcsec for 1mm crystals and 30–40 arcsec for 1–3 mm ones. For larger platelets the rocking curves often split into a few $\sim$ 30–40 arcsec peaks showing a presence of low angle (1–3 arcmin) boundaries separating grains of a few mm in size. Misorientation between grains increases monotonically from end to end of the crystal [51]. It has been suggested that this can be also related to the polar character of the platelets growth leading to some strain and its subsequent relaxation through the formation of the low angle boundaries.

TEM examination by Liliental-Weber *et al.* [38] showed that the N-polar $(000{-}1)$ surface of the n-type pressure grown GaN crystals (especially for the smaller ones) is frequently atomically flat (2–3 single atomic layer steps on the surface) and that the crystals under this surface are practically free of extended defects. Below the opposite, rough surface, a number of extended defects such as stacking faults, dislocation loops and Ga microprecipitates can be found. The relative thickness of this part usually consists of 10% of the entire thickness of the platelet. It seems that the presence of these defects is related to the growth instabilities often observed on the Ga-polar surface of the crystals grown without an intentional doping.

For the use of the crystals as substrates for epitaxy, the near surface part of the material being often the result of the unstable growth has to be removed by polishing and subsequent Reactive Ion Etching (Ga-side) or mechano-chemical polishing (N-side). As a rule the extended defects are not observed by TEM in the crystals used as substrates for both N and Ga polarity epitaxial growth. Therefore, if the epitaxy is properly performed, both the substrate and the layer quantum structure are free from dislocations that can be observed by TEM.

Unfortunately, the TEM technique allows to analyze only a very small area samples. Therefore, in order to measure dislocation densities in GaN, the Defect Selective Etching (DSE) methods have been developed [55]. It was shown that etching in molten KOH-NaOH eutectics reveals dislocations in both GaN heteroepitaxial layers and GaN pressure grown single crystals. Fig. 14(a) shows the result of DSE of typical GaN heteroepitaxial layer grown by MOCVD on sapphire substrate. High density of the etch pits are shown. The same method applied for bulk crystals gives very small (10–100 cm^{-2}) number of the etch pits. The typical pit observed on both heteroepitaxial layers and crystals is shown in Fig. 14(c). The pattern in Fig. 14(b) is the result of DSE of GaN single crystal with dislocations generated intentionally by indentation with diamond. The etch pits surround the imprint of the diamond showing the area where dislocations are present and that the remaining material is dislocation free.

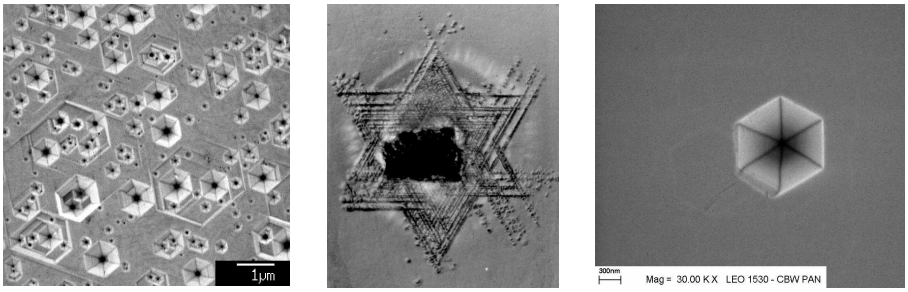


Fig. 14. Defect Selective Etching of GaN: a — GaN/sapphire heteroepitaxial layer after etching in molten KOH-NaOH eutectics [55], b — GaN pressure grown single crystal after indentation with diamond and etching in molten KOH-NaOH eutectics [54], the average size of the star like pattern is 100 mm, c — etch pit (EP) on the GaN crystal surface after etching in molten KOH-NaOH eutectics [55], observed density of EP — 10–10^2 cm^2.

3. Epitaxy and devices

3.1. Introduction

The spectacular development of GaN-based optoelectronic devices was possible due to elaboration of the two-step Metal Organic Vapor Phase Epitaxy (MOVPE) process for the growth of (GaAlIn)N epitaxial structures on highly mismatched sapphire substrates. In these structures dislocation densities are as high as 10^8–10^{10} cm^{-2} but, nevertheless, very efficient luminescence is possible if the structures contain InGaN [1].

Nakamura suggested that this is due to strong localization of carriers in deep potential wells caused by compositional fluctuation in InGaN alloys [1], which localized the carrier far away from the dislocations and hampered their role as nonradiative recombination centers. However, for high injection currents (*i.e.* in high power LDs), the potential minima are too shallow to contain all the injected carriers and therefore for lasers, the reduction of dislocation density in the material is much more important than for LEDs. The Nakamura's model explains in a consistent way the following characteristics of Nichia optoelectronic devices (both LEDs and LDs) :

- The nitride LEDs containing In in their active structures are much more efficient than LEDs with pure GaN active layers (not alloyed with In).
- InGaN LEDs efficiency does not depend critically on dislocation density (if Al_2O_3 or ELOG are used) in contrast to the efficiency of In-free UV diodes.
- At high injection currents, the high dislocation density lowers the efficiency even for InGaN LEDs.

Therefore, one can expect that the elimination of dislocations from the structures should lead to:

- High efficiency In-free UV LEDs.
- Higher efficiency and higher power of both UV and visible laser diodes than it is possible with dislocated structures.
- Reduction of the dislocation-related strain in the LD structures.
- Possibility of the reduction of the growth temperature.
- Investigation of p-doping by the use of higher content of Mg.

In the following both In-free and In-containing structures are considered and the results supporting the above expectations are presented.

Crystal growth of dislocation-free nitride structures requires surface preparation. Due to the different chemical properties of the Ga-side and the N-side surfaces, the different surface preparation techniques were developed.

The initial step of the preparation of both sides of GaN plate-like crystal relies on mechanical polishing of the crystal. The polishing has to remove the surface layer of the GaN crystal which usually contains higher amount of oxygen and frequently has additional impurities. This layer is grown during the last stage of HP growth, *i.e.* during cooling down of Ga solution under high nitrogen pressure. In addition, this procedure served to obtain the standard and uniform thickness of the substrate, which is very important for the processing of the laser structures. Also it is possible to obtain the designed misorientation of the substrate in order to assure the best growth of the epitaxial layers.

Since the N-side of GaN surface is chemically active, the subsequent stage of GaN surface preparation is by mechano-chemical polishing. It has been showed that simple chemical etching of the N-side of GaN crystals in KOH 1:5 (1 weight part of KOH is dissolved in 5 weight parts of water) led to creation of hill and valley structure [55]. The etching slows down after 5–7 minutes and is virtually negligible after 20 minutes. After 5 minutes the skeleton of pyramidal structure is emerging. After 50 minutes of etching a full pyramidal structure was developed. It is likely that the protective chemically inert, insoluble oxide layer is created and the etching process is stopped. From the AFM image of this structure it was deduced that the etching ends when the [10−12] faces of the opposite polarity are totally exposed.

By simultaneous mechanical polishing and chemical etching the chemical process is greatly enhanced. As shown by AFM measurements, the process can be continued until the creation of perfectly flat surface [57]. The RBS measurements showed that the subsurface layer is free of the defects introduced during mechanical polishing stage [57, 58].

In contrast to the N-side, the Ga-side of GaN plate-like crystals is much more chemically inert. This is particularly unfortunate because only the growth on the Ga-side allows to obtain optically active structures necessary to effective optoelectronic devices (LEDs and LDs). The growth on the N-side has not led to creation of effective LEDs or LDs. The advantage of Ga-terminated (0001) face stems from more effective incorporation of acceptors than N-terminated (000−1) face. On contrary, N-terminated face easier incorporates donors, also impurities, like oxygen [59]. Preparation of the Ga-side can be made using more aggressive etching agent which requires

protection of more active N-side that is technically difficult. Alternative way is to use reactive ion etching (RIE) to remove the mechanically damage subsurface layer. This technique has been developed [60], in which GaN is etched using Cl ions. The chlorine ions bombardment results in formation of volatile Ga-Cl species. It this way the damaged layer is removed, but the surface morphology is still far from being the flat surface, necessary for high quality epitaxial growth. Then by annealing in ammonia and hydrogen mixture this surface structure is removed and the surface is suitable for epitaxy. Typically these annealing processes are performed in the apparatus used in MOVPE.

3.2. Metalorganic chemical vapor epitaxy (MOVPE) on GaN substrates

Metalorganic chemical vapor epitaxy is the most widely used technique for growing III-N nitride layers. The MOVPE results reported here were obtained in IHPP using vertical flow reactor. The gases (N_2, H_2 and NH_3) are purified to ppb level by SAES getter purifiers. The following metal-organic compounds are used: TMG, TMA, TMI as source of group III metal for growing (Al,Ga,In)N layers, Cp2Mg for Mg-doping, SiH_4 for Si-doping. The substrate is heated by an inductive coil that enforces current flow in a graphite (SiC-coated) susceptor.

The growth is monitored by laser reflectometry. A typical time variation of the reflected light intensity, obtained during the growth of InGaN based laser-structure, is presented in Fig. 15. Each oscillation corresponds to change of the thickness of about 1300 Å. The diagram shows that during a very complicated growth (more than 100 different layers) the amplitude of oscillation remains almost constant for the same chemical composition, which indicates that the surface roughness was not increased. Using laser reflectometry, it is possible to monitor the growth with 2–3 Å accuracy, what is necessary for the precise determination of the width of the multiple quantum wells (MQW) structure.

If the surface preparation and the conditions of the epitaxial growth allow growth by undisturbed step flow mode, the structure of GaN homoepitaxial layers, in terms of dislocation density, follows the structure of the GaN substrates. Fig. 16 shows the AFM results demonstrating the difference in the surface morphology of GaN epitaxial layers deposited by MOVPE in the same run, on GaN crystal and on GaN/sapphire substrate.

The atomic step flow on the surface of the homoepitaxial (GaN/GaN) layer is not perturbed in contrast to the noisy pattern measures after deposition of GaN layer on GaN/sapphire substrate containing high density of threading dislocations. The dislocations disturb the atomic step flow leading to entangled step structure shown in Fig. 16(b). In case of high quality epi-

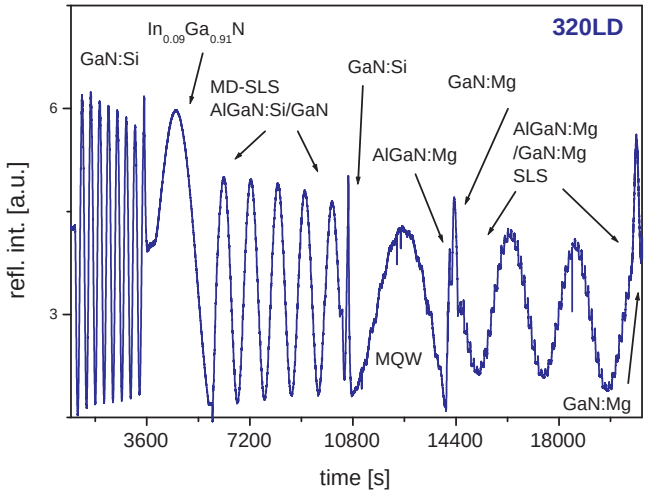
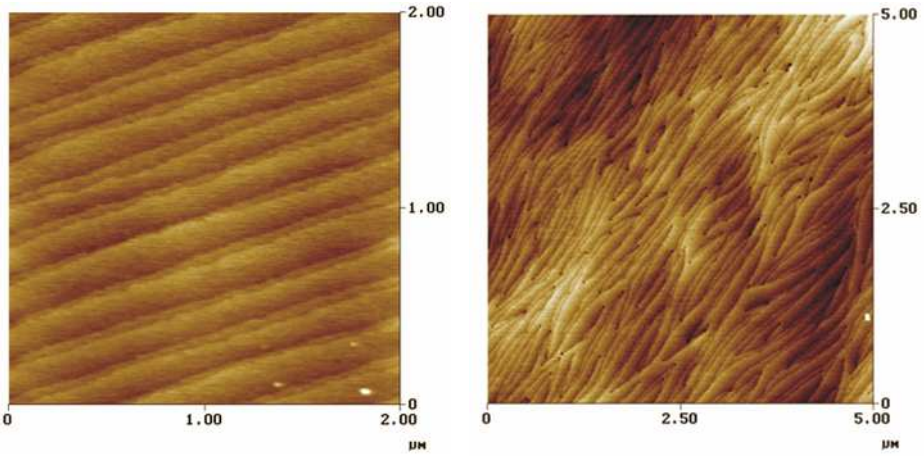


Fig. 15. Optical reflectance measured during growth of quantum structure by MOVPE. Note the short change of reflectance corresponding to growth of multiquantum well (MQW) structures and AlGaN/GaN superlattice structures (SLS).

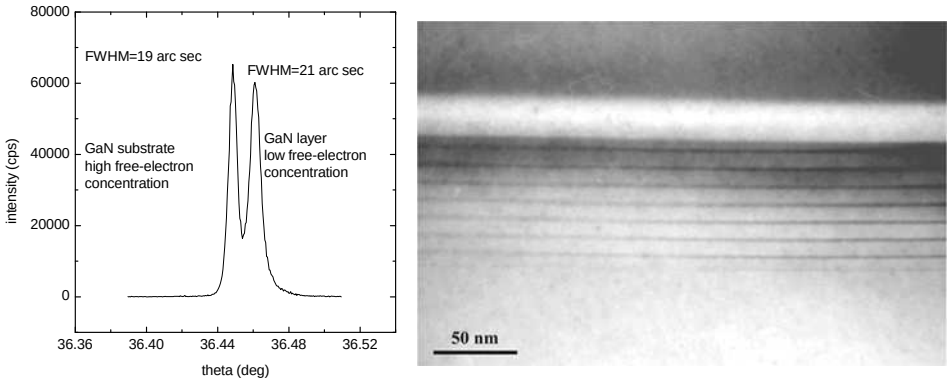


(a) (b)

Fig. 16. Surface morphology of GaN epitaxial layers deposited by MOVPE on different substrates: (a) — GaN pressure grown crystal, (b) — sapphire.

taxial growth, proceeding by parallel step flow as demonstrated in Fig. 16(a), the homoepitaxial GaN layers reproduce crystallographic quality of the substrates. Fig. 17 presents the X-ray diffraction rocking curve measured on GaN/GaN structure that has two intensity peaks corresponding to the GaN substrate grown at high pressure (HP-GaN) and the homoepitaxial layer,

respectively. Both peaks have FWHM (full widths at half maxima) of about 20 arcsec, the value to be obtained for a perfect GaN crystal examined using this XRD system. The peaks are separated indicating that the lattice of the GaN bulk crystal is slightly expanded by high density of the free electrons and point defects [61]. FWHM of the bound exciton lines less than 0.5 meV is observed for layers grown by MOCVD (*i.e.* [62,63]) on the Ga-polar surfaces of the GaN substrates.



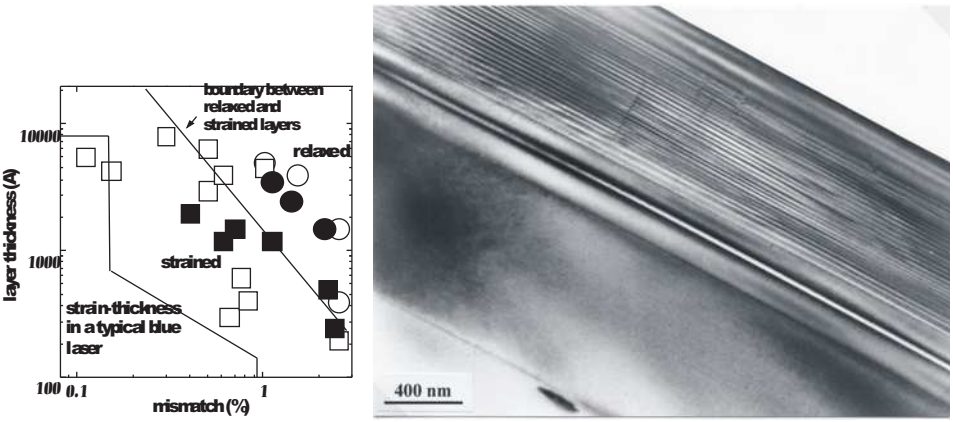
(a) (b)

Fig. 17. (a) — X-ray diffraction rocking curve of MOVPE grown GaN homoepitaxial undoped layer and the HP *n*-type GaN substrate. (b) — InGaN MQW grown on the Ga-polar (0001) surface of GaN substrate by MOVPE, TEM — courtesy of M. Albrecht.

The InGaN near dislocation free epitaxial layers and quantum wells were grown by MOVPE, on the pressure grown crystals, in the Institute for High Pressure Physics by Leszczynski *et al.* [60]. In Fig. 17(b) the Transmission Electron Microscopy (TEM) image of one example of the InGaN MQWs structure is shown. The TEM images prove that in these structures the density of dislocations is too low to allow the observation of the dislocations in relatively small area TEM scan.

Dislocations in the structures grown on the almost dislocation-free GaN substrates can appear as a result of the lattice mismatch between GaN and its ternaries: InGaN and AlGaN. This was analyzed by Leszczynski *et al.* [64] by the X-ray measurements of lattice parameters of various GaN-based epitaxial layers deposited on GaN substrates as a function of the InGaN (or AlGaN) layer composition and thickness. It was shown that the boundary between fully strained and relaxed InGaN (AlGaN) layers is in a safe distance from mismatch — thickness area for layers necessary for a typical blue laser structure. These results are collected on the diagram in Fig. 18(a).

Fig. 18(b) shows an example of the multilayer structure similar to the full structure of blue laser. The example confirms that no mismatch dislocations are generated if the structure is grown on dislocation free GaN substrate.



(a) (b)

Fig. 18. Critical conditions for III-N ternaries: (a) — X-ray data: open circles — AlGaN relaxed, open squares — AlGaN strained, filled squares — InGaN strained, open squares — InGaN relaxed, (b) — TEM image of the multilayer structure deposited on GaN substrate by MOCVD, the sequence of layers from the lower left corner: n-GaN, n-$Al_{0.11}Ga_{0.89}N$/n-GaN superlattice, n-GaN, $In_{0.09}Ga_{0.91}N$, p-GaN, p-$Al_{0.14}Ga_{0.86}N$/p-GaN superlattice, p-GaN.

TEM and AFM techniques can probe only an area of a few square microns. Using XRD we examined an area of a few millimeters squared. Fig. 19 presents an experimental scan for a laser structure compared with a theoretical simulation using a dynamical X-ray diffraction theory.

For GaN and AlGaN layers (on the right-hand side of the scan), the peaks are very narrow, not broadened by compositional fluctuations. For InGaN, as expected, the peaks are slightly broader than for a perfect structure.

Even when dislocation-free GaN substrates are used, the LD structure contains highly lattice-mismatched parts of AlGaN and InGaN that can be relaxed by dislocations. It follows from the defect selective etching that the rate of etching is different for layers of various chemical composition which allows to determine where the dislocations originate. This knowledge is crucial and serves as convenient tool in optimizing the deposition of the LD structure.

The etching experiments were performed in the modified molten bases system [65] in the temperature 450°C, for 40 minutes in order to determine the layer of the laser structure where the dislocations emerge. The etched samples were examined by the scanning electron microscopy (SEM),

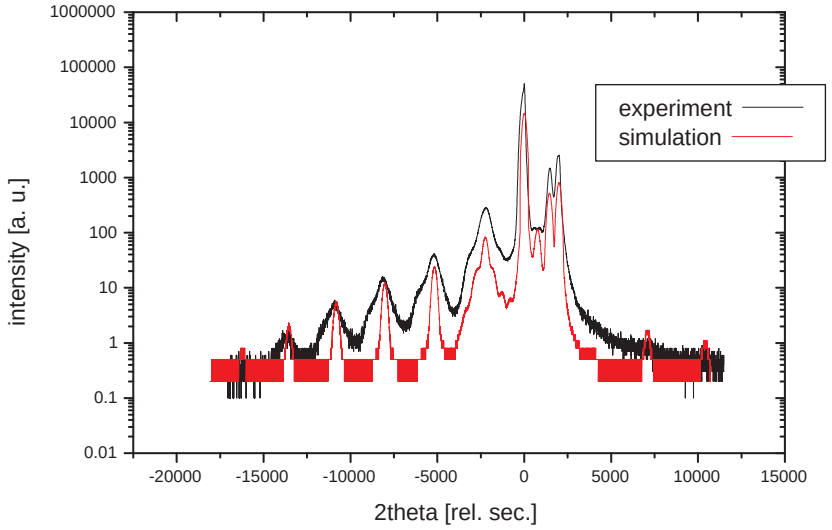


Fig. 19. X-ray scan of laser structure. For comparison an X-ray intensity of simulated perfect structure is presented.

transmission electron microscopy (TEM) and optical microscopy with differential interference contrast (DIC). The morphology of the etch pits was determined by the AFM method. 3D etch pits maps and cross sections were obtained. The results of these measurements indicate that the two classes of the dislocation were discovered [65]. The first class consists of the dislocations generated in the p-type GaN below the upper cladding. The second class are the dislocations which started at the InGaN MQW. In order to confirm the dependencies between the structure of the laser and the etch pit shape, the TEM investigations were performed. The results of these TEM measurements confirmed the classification based on AFM results.

The differences in the etch pit shapes allow fast determination of the place where the dislocations were generated. Hence for the large area investigations the AFM study is not necessary. The approximate measurements of the pits depths may be based on the SEM images. Presented in Ref. [65] is the example of the area of 6×10^4 μm^2, where only 8 etch pits of the first class were discovered. There were also 35 pits of the second class giving 63 pits in total. The pits distribution on this sample surface seems to be homogenous, so these results can be used for the estimation of the etch pits densities for the whole sample. The total etch pits density was 1.05×10^5 cm^{-2}. The densities of the pits associated to the dislocations starting above the MQW, in the MQW and below the MQW were estimated to be 1.3×10^4, 5.8×10^4 and 3.3×10^4 cm^{-2}, respectively.

In all LDs the active part of the device is composed of one to five $In_xGa_{1-x}N$ quantum wells of a width of 40 Å (x varies between 0.02 and 0.15 for 380–430 nm devices). The quantum barriers are $In_{0.02}Ga_{0.98}N$:Si layers of a thickness of 70 Å (for 415 nm and 430 nm devices) and quaternary InAlGaN layer for 380 nm diode. The quantum well system is followed by a 200 Å-thick $Al_{0.2}Ga_{0.8}N$:Mg electron blocking layer, 0.07 μm-thick undoped upper and 0.1 μm-thick n-type lower GaN layer form the device waveguide. A 0.5 mm-thick n-type $Al_{0.16}Ga_{0.84}N$/GaN superlattice (110×24 Å/24 Å) was used as bottom cladding and 0.37 μm-thick p-type $Al_{0.15}Ga_{0.85}N$/GaN superlattice (80×23 Å/23 Å) as upper cladding to confine the light emitted from the active region of the InGaN MQW structure. A 40 nm-thick p-type GaN layer was used as a contact layer of the p-electrode.

The devices were processed as ridge-waveguide, oxide-isolated lasers. The mesa structure was etched out in the wafer down to a depth of 0.3 μm (roughly to the middle of the upper cladding layer). The laser structure was then isolated by the e-beam deposition of a 0.1 μm layer of ZrO_2. Ni/Au contacts, of typical contact resistance between 10^{-3}–10^{-4} $\Omega \times cm^2$ (measured for low currents), were deposited on the top surface of the device, while Ti/Au contacts were deposited on the backside of the highly conducting n-GaN substrate crystal. The stripe width was set to 20 or 50 μm and the resonator length was 500 or 1000 μm. The mirrors were coated with quarter-wavelength layers of SiO_2/TiO_2 to increase the mirror reflectivity. The structures were characterized by a density of dislocations at the level of around 10^5 cm^{-2}. Most of these dislocations were initiated in the upper part of the structure, especially in electron blocking layer.

Figure 20 presents the dependence of the threshold current density on the laser emission wavelength. The minimum current is achieved for 415 nm device while for 380 nm and 430 nm lasers we observe a certain increase of the lasing threshold. However, one has to remember that 415 nm lasers have undergone much longer optimization process [67].

The emission spectra of all lasers have multimode character and average linewidth of 0.5–1.5 nm. The 415 nm laser diode (stripe width 20 μm) was able to emit up to 180 mW of total power (both facets) as it is shown in Fig. 21 [67].

The main limitation for the operation of these devices is the thermal roll-off of the L-I characteristic. The L-I curve of large area 20×1000 μm^2 ($\lambda = 415$ nm) laser was measured [63]. The threshold current for this device is satisfactory (1 A which corresponds to 4 kA/cm^2 of the threshold current density). The electrical power at the threshold is equal to 7 W. The roll-off current in that case is 1.35 A . One should take into account also that the differential efficiency for CW and pulse laser is much higher for the latter one (0.176 W/A as compared with 0.28 W/A for pulse operation). That

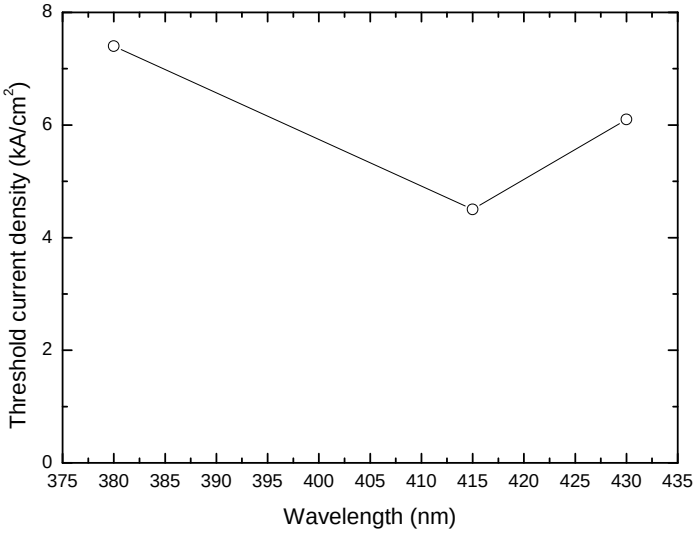


Fig. 20. The dependence of threshold current density on the emission wavelength for wide stripe (20 μm) laser diodes.

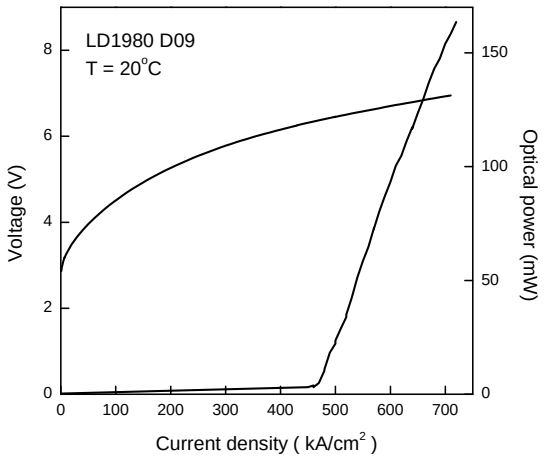


Fig. 21. Light-current and current-voltage characteristics of 415 nm laser diode measured at room temperature.

means that the heating is substantial for all values of the operating current. In order to optimize thermal properties of this laser we will measure the temperature of laser chip/diamond/radiator system in order to establish the most critical regions of high thermal resistivity.

One of the most important issues related to the operation of nitride laser diodes is the successful removal of the large amount of heat dissipated during diode operation. Nitride laser diodes are characterized by a ten-fold larger threshold current density and threshold voltage two times larger as compared with their GaAs counterparts. This results in a more than 20 times higher electrical power consumption at threshold comparing with GaAs based devices. In case of our wide-stripe laser we have the electrical power density at threshold in the range of 24–30 kW/cm^2.

Here we report data on the three types of wide-stripe:

— Type A: laser with a 20 μm $\times$ 500 μm stripe.

— Type B: laser with a 20 μm $\times$ 1000 μm stripe.

— Type C: laser with a 50 μm $\times$ 500 μm stripe.

All these diodes were mounted p-side down on metalized diamond heat-spreaders. The electrical parameters of these devices are listed in Table II.

TABLE II

Electrical properties of different types of GaN based homoepitaxial lasers.

Laser type	I_{thr} (mA)	J_{thr} (kA/cm^2)	V_{thr} (V)	Maximum current at CW operation (mA)	Emitting wavelength (nm)
20 μm $\times$ 500 μm	395–550	3.95–5.5	6.2–6.7	1300	412–415
20 μm $\times$ 1000 μm	1000–1300	5–6.5	6.8–7.1	1900	405–420
50 μm $\times$ 500 μm	1296–1722	5.2–6.9	7–8	Not tested	402–415

As it is shown in Table II, these devices are characterized by similar parameters in terms of threshold current density and threshold voltage, which implies that the device current remains proportional to the stripe area. The dissipated power varies roughly between 2.5 W and 8 W, depending on the stripe geometry. This large amount of heat forces us to use an active thermoelectric cooling system. Our measurements indicate that the temperature roll-off of L-I characteristics occurs for an electrical power density of 80 kW/cm^2.

The optical and electrical characteristics under CW operation of lasers "A" and "B" were measured. Their performance seems to be similar. So far slightly higher optical output powers were achieved by using a 20 μm device. The maximum ratings of our lasers are so far limited by the slope efficiency and by the thermal resistance of the package, which should both be improved.

So far, laser "C" was not successfully tested under CW operation because of thermal management problems. However, we believe that, with an improved mounting scheme, this type of laser may provide a good solution for the 1 W emission range.

Fig. 22 shows the pulsed current test performance of a class "A" device. We could demonstrate over 2.5 W of optical power on the output mirror. The failure of this device for larger power coincides with the COD level (50 MW/cm^2). We expect that type "C" devices would be able to emit over 5 W of radiation from a single stripe (at least under pulse operation). The maximum optical power obtained without failure was 2.7 W measured from the front mirror of the laser. That proves that very wide-stripe nitride lasers may reach 3–5 W of optical power from the single stripe beating the standard phosphides and arsenides devices.

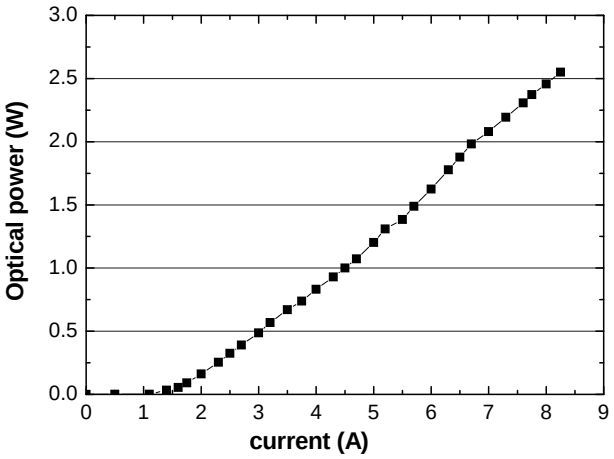


Fig. 22. Light-current characteristic measured under pulsed current conditions (5 kHz, 20 ns). Highly reflective coating causes almost all emission to exit through the output mirror.

The beam quality of conventional high-power laser diodes is usually hampered by the multi-mode character of their emission which leads to deteriorated M^2 values of these devices. In order to combine highpower and good single-mode operation we used an external cavity scheme (Littrow configuration). Using an external cavity we narrow down the laser spectrum and we also gain additional possibility of wavelength tuning using the external grating. Figure 23 shows the results of laser tuning. We demonstrate over 4 nm of tunability of such a laser without using AR coatings, which compares well with the previous literature values obtained for narrow stripe diodes. This latter experiment was performed on a pulse operated laser and experiments with CW operated devices are in progress.

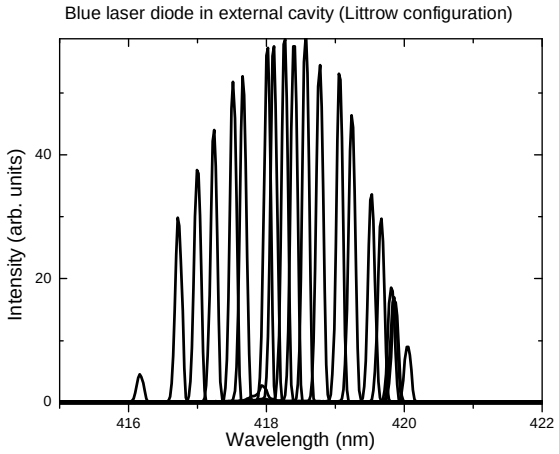


Fig. 23. The spectra of laser emission obtained in the Littrow external cavity configuration, for different grating angles.

3.3. Molecular beam epitaxy

Molecular beam epitaxy (MBE), which in principle gives more precise growth control, until recently lagged considerably behind MOVPE in the field of nitride based optoelectronic devices [69, 70]. These difficulties were often explained by using thermodynamic argument which sets the optimum temperature for epitaxial deposition to about $0.5 \times T_{\mathrm{M}}$, where T_{M} is the melting temperature of the material in question. According to such estimates, growth at much lower temperatures results in poor adatom kinetics, which leads to 3D growth mode and rough surfaces. For GaN experimentally determined T_{M} is 2540 K (for 6GPa) [3] and theoretically predicted 2800 K [20], which would set the minimum temperature for good epitaxy to about 1300 K–1400 K (1000°C–1100°C). However, in the vacuum, GaN starts decomposing at temperatures already well below 800°C. Further increase of the temperature accelerates decomposition rate exponentially and matching overpressure of active nitrogen species is needed to stabilize the surface and to promote the growth of the layer. In MOVPE, ammonia overpressure in mbar–bar range prevents GaN decomposition for temperatures in excess of 1000°C. Clearly for MBE, which relies on the negligible interaction of the atomic beams, such conditions are unattainable. Still, some groups working in the nitrides managed to push the growth conditions in the MBE reactors fairly close to these used in the MOVPE by growing at temperatures as high as 950°C with the use very high ammonia flows (up to 200 sccm). Owing to the nitrogen precursor used, this technique is often referred to as ammonia MBE. Recently, after several years of optimizing this technology,

Hooper *et al.* [71] from Sharp Laboratories of Europe demonstrated the first MBE grown "violet" LDs, operating at room temperature under pulsed conditions. In spite of its potential advantages for both optoelectronic [71] and electronic [72] devices, ammonia MBE has not been the technique of choice for the majority of nitride MBE community. Indeed, the corrosive nature of ammonia compounded by its large flows creates additional hazards and technological challenges as well as leads to often undesirable high hydrogen background during the epitaxial process. In the more widely employed plasma assisted MBE (PA-MBE) [72], purified nitrogen gas is activated using an RF-plasma and supplied to the growing surface at typical flow rates of 1–2 sccm. The technique already proved its potential for the growth of high quality structures for electronic components [73], but until now only limited success was reported in the area of optoelectronic devices [74]. The turning point for GaN growth with PA-MBE was the discovery that Ga rich conditions are necessary for growth of high quality GaN and AlGaN/GaN heterostructures. High quality layers and interfaces were demonstrated at temperature range of 650–750°C, much lower than required for the growth of similar structures with ammonia [75–79]. In our earlier works we optimized the growth conditions for high quality GaN and AlGaN/GaN heterojunctions in Ga rich regime, and demonstrated *(i)* the record high electron mobility of two-dimensional electron gas at the AlGaN/GaN interface and *(ii)* very narrow photoluminescence lines from GaN epitaxial layers [62, 63]. Extensive study of the growth of nitride structures with In as the surfactant enabled us to grow first InGaN LDs by PA-MBE [80]. Recent *ab initio* calculations explain that smooth, step-flow growth of GaN (AlGaN, InGaN) achieved at relatively low temperatures is possible because of existence of a very efficient lateral diffusion channel for adatoms on semiconductor surface just below the dynamically created thin (two or one layer) Ga or In film [81–83]. Surprisingly small activation energies for this so called adlayer enhanced lateral diffusion (AELD) enable high quality epitaxy at temperatures much lower than expected from mentioned earlier estimates based on GaN melting point. In this work, we investigate parameters of LDs with different number of InGaN QWs grown by this new PA-MBE technique.

The LDs structures were grown in custom designed V90 VG Semicon based MBE system (now Oxford). Ultra-high purity gas handling manifold together with Veeco UniBulb RF Plasma cell was used as a source of activated nitrogen. The LDs structures were deposited on conductive, very low dislocation density, high-pressure-grown GaN bulk substrates [4]. The epi-ready bulk substrates were prepared in the three-step process of mechano-polishing, dry etching and deposition of 2 μm GaN:Si buffer layer in the MOVPE reactor. The back sides of the substrates were coated with 0.7 μm of molybdenum layer to improve the thermal coupling for radiative

heating. Special holders capable of accommodating small irregularly shaped substrates (5×5 to 10×10 mm approximate size) and designed to minimize edge effects ensured high temperature uniformity across the entire substrate area. The LDs structures consisted of the following sequence of layers: the 200 nm of GaN:Si buffer layer was followed by 0.55 μm $Al_{0.08}Ga_{0.92}N$:Si cladding layer. The wave guide was asymmetric with lower part consisting of 100 nm GaN:Si and 40 nm $In_{0.01}Ga_{0.99}N$:Si. Depending on the structure, five, three or two undoped 4 nm thick $In_{0.09}Ga_{0.91}N$ Quantum Wells (QW) with 7 nm $In_{0.01}Ga_{0.99}N$:Si barriers were deposited in the active region. 14 nm $In_{0.01}Al_{0.16}Ga_{0.83}N$:Mg blocking layer was followed by 70 nm $In_{0.01}Ga_{0.99}N$:Mg upper wave guide. The upper cladding consisted of 80 pairs of uniformly Mg doped $In_{0.01}Ga_{0.99}N/In_{0.01}Al_{0.16}Ga_{0.83}N$ short period superlattice (2.5/2.5 nm). The contact layer was 100 nm GaN:Mg or InGaN:Mg. Doping levels for n-type layers was 5×10^{18} cm^{-3}, while hole concentration obtained from Hall effect measurements on a reference 0.3 μm thick $In_{0.01}Ga_{0.99}N$:Mg layer was 2×10^{18} cm^{-3}.

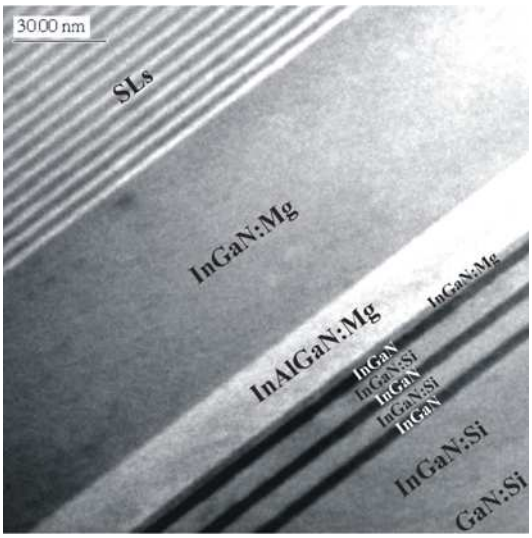


Fig. 24. TEM picture of 3QWs laser diode structure.

The growth temperature for GaN and AlGaN layers was 710°C (growth at Ga-rich regime), while QWs and p-type cladding were grown at 590°C (growth at In-rich regime). To enable high quality growth, the excess Ga and In fluxes were precisely chosen to form dynamically stable metal film on semiconductor surface which enhance lateral adatom mobility [78, 81]. We used solid sources (high purity Si and Mg) for n and p type doping. No post growth annealing was necessary to activate p-type conductivity. In

Fig. 24 we show state of the art of the PA-MBE technology — transmission electron microscope (TEM) picture of laser diode structure containing 3 InGaN/InGaN QWs.

The laser diode devices were processed as ridge-waveguide, oxide-isolated laser. The mesa structures were etched out in the wafers down to a depth of 0.35 μm. The laser structures were then isolated by e-beam deposition of a 0.2 μm layer of SiO_x. The final devices had the stripe width of 15 μm and the resonator length of 500 μm. The oxidized Ni/Au ohmic contacts were deposited on the top surface of the devices, while Ti/Au contacts were deposited on the backside of the highly conducting n-GaN substrates. The tested devices had cleaved uncoated mirrors.

The lasers operation was demonstrated at room temperature using 50 ns pulses at 0.25% duty cycle. Fig. 25 presents the light-current-voltage (L-I-V) characteristics for typical LDs. A sharp increase of the light power visible at the current of about 1 A and 9 V bias is indicative of the laser operation. The lowest threshold current obtained for our lasers was 680 mA (at 8.2 V bias) which gives threshold current density of 9 kA/cm^2. The slope efficiency per facet calculated from L-I plot was 0.35 W/A for 5 QWs and 0.47 W/A for 2 QWs device . The maximum output optical power was measured to be 1.1 W for the LDs with 2 QWs. Strong narrowing of the spectral line was detected above the threshold current (see Fig. 26). For this device multimode lasing was observed at 408 nm with mode spacing close to 0.53 Å, which indicated the presence of longitudinal modes. The total linewidth of emission is close to 0.4 nm. We would like to point out that threshold currents and voltages for 2 and 5 QWs LDs are very similar. Since other device parameters are not changed, this result might indicate that only two quantum wells contribute to the lasing operation for the five QWs device, pointing towards possible structure design issues. In fact, the parameters of our laser diodes, the output power in particular, are as good as the early MOVPE LDs or better.

The very important factor responsible for laser diode parameters is p-type doping. Effective p-type doping of GaN is still a subject of intensive studies because it is crucial for nitride-based LEDs and LDs. The low electrical activation of Mg acceptor in GaN, due to its high ionization energy, requires very high doping level of Mg to obtain desirable hole concentrations. It was already reported that growth of GaN:Mg by PA-MBE resulted in high p-type conductivity without any post growth annealing and with very sharp Mg doping profiles [84–86]. Systematic study of the Mg doping of GaN by Smorchkova *et al.* [84] showed that for the constant growth temperature, Mg flux controls p-type conductivity. The hole concentration as high as 1.3×10^{18} cm^{-3} was achieved for Mg doping of 10^{20} cm^{-3}. As it was shown by Haus *et al.* [85], growth at low temperatures increases Mg sticking coef-

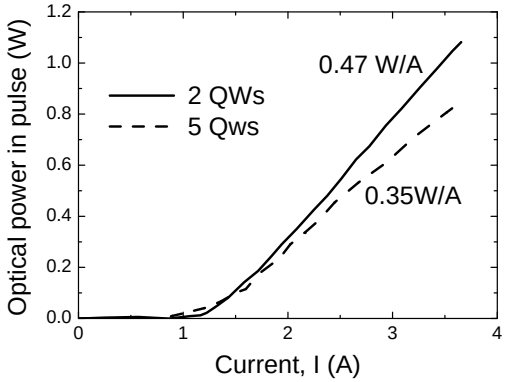


Fig. 25. Light–current characteristics for 2 (solid line) and 5 (dashed line) InGaN/InGaN QWs laser diodes grown by plasma assisted molecular beam epitaxy. Laser diodes were operated at pulse mode.

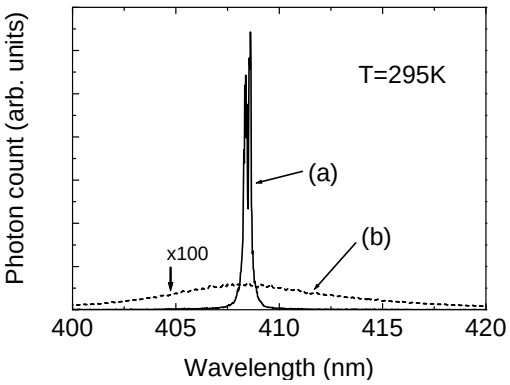


Fig. 26. The emission spectra of laser diode operating below (b) and above (a) lasing threshold for 5 InGaN/InGaN QWs laser diodes.

ficient considerably which can be an efficient method to achieve higher Mg doping level. However, as it was pointed out there, the Mg atoms enter GaN layer for Ga or N rich conditions at the same level, but for N rich regime, the Mg acceptors can be compensated by the presence of donors like Ga vacancies mainly due to the low quality of grown layers. For very high Mg flux, when the Mg surface coverage is about 1 ML, the polarity inversion (PI) from Ga to N on GaN layer can take place [87–89], which leads to the abrupt decrease of the Mg doping efficiency and deteriorate dramatically crystal quality. Therefore, the PI effect is a main limiting factor in achieving high Mg content in GaN layers.

The hole concentration was measured at the hall bar geometry samples prepared by reactive ion etching on layers grown on GaN/sapphire templates. A 10nm/20nm Ni/Au contacts were annealed at 450°C for 10 minutes at oxygen atmosphere. The maximum measured hole concentration for GaN:Mg was 5×10^{17} cm^{-3} with mobility 7 cm^2/Vs for Mg concentration 10^{20} cm^{-3} (see dots in Fig. 31). The p-type hall conductivity depends on the Mg acceptor activation energy E_{A}, the number of Mg acceptors $\mathrm{N_{Mg}}$ and the number of compensating donors N_{D}. In Fig. 27 we plot the concentration of holes as a function of the Mg acceptors. Solid points show the results of our experiments, while solid and dashed lines are calculations according to neutrality equation with acceptor ionization energy $E_{\mathrm{A}} = 200$ meV and compensating donor concentrations $N_{\mathrm{D}} = 0$ and $N_{\mathrm{D}} = 10^{18}$ cm^{-3}, respectively [90]. For modeling we use hole effective mass $m^* = 1$.

There is still an animated discussion about the Mg activation energy and the values and the impact of the InGaN:Mg to the maximum p-type conductivity. Due to the lower hole effective mass in InGaN, the acceptor activation energy E_{A} should be smaller giving in turn more holes in valence band for the same doping level in comparison with GaN. In addition, localization effects present in InGaN can strengthen this trend. Indeed, in our PA-MBE InGaN:Mg layers we observe substantial increase of the hall concentration for the same Mg concentrations measured by SIMS — see squares at Fig. 27. The maximum hall p-type concentration was found at the level 2–4 $\times 10^{18}$ cm^{-3}.

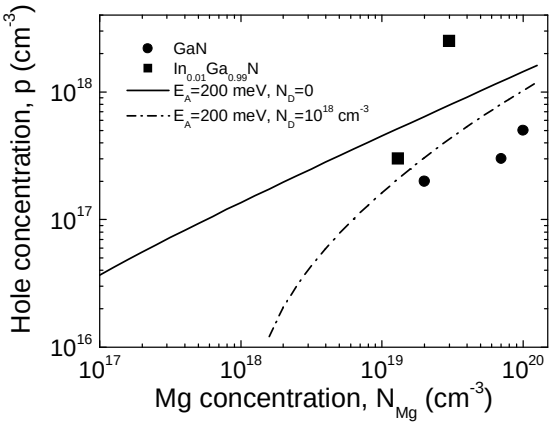


Fig. 27. The hole concentration as a function of the Mg acceptor content. Dots and squares are experimental points for GaN and InGaN, respectively. Solid, and dotted-dashed lines are calculations for acceptor activation energy $E_{\mathrm{A}} = 200$ meV, and compensating donor concentrations $N_{\mathrm{D}} = 0$ and $N_{\mathrm{D}} = 10^{18}$ cm^{-3}, respectively.

Other crucial elements in this work was optimization of the optical quality of the quantum wells by fine-tuning the growth parameters to maximize the room temperature photoluminescence (PL) intensity and to minimize full width at half maximum (FWHM) of the PL lines. We find that peak PL intensities for our optimized test 10-period $In_xGa_{1-x}N/In_{0.02}Ga_{0.98}N$ MQW structures grown on bulk GaN substrates cover spectral range from 385 to 530 nm, *i.e.* energy from 2.4 eV to 3.3 eV (see Fig. 28). Equally important are very small values for FWHM of the measured PL lines, varying from 7 nm (for PL line at 385 nm) to 35 nm (for PL line at 530 nm) with increasing In content in the QW from 5 to 27%. The FWHM can be influenced by a number of factors, such as uniformity of In composition in the wells, uniformity of In composition from well to well and the quality of the interfaces.

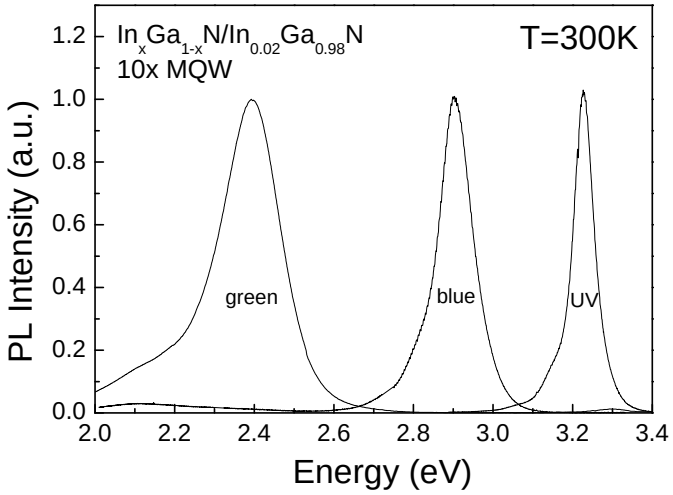


Fig. 28. Photoluminescence spectra of $In_xGa_{1-x}N/In_{0.02}Ga_{0.98}N$ multiquantum wells at $T = 300$ K.

By engineering the quantum confinement properties of electrons on a nanometer scale in GaN/Al(Ga,In)N quantum wells, it is possible to develop devices relying on intersubband (IS) absorption or emission at 1.3–1.55 μm telecom wavelengths. Therefore, it allows to move nitride based emitters into infrared region. The operating principles of IS devices have already been successfully validated at mid- and far-IR wavelengths in using semiconductor materials such as GaAs/AlGaAs or InGaAs/AlInAs-on-InP [91, 92]. The main technological problem in nitride based devices lies in the difference in lattice constants between GaN and AlN. The practical realisation of GaN/AlN MQW devices leads to lattice relaxation and subsequent formation of cracks and large number of defects. Since InN has larger lattice

constant than GaN incorporation of In to AlN (in proportion 17% In 83% Al) gives InAlN lattice matched to GaN [93]. However, the band offset for such system is too small to reach 1.55 μm IS absorption. Therefore we have grown barriers with higher Al content (93%–96%). To make full advantage of the GaN substrates we have grown strain compensated AlInN/InGaN MQWs. The $In_{0.05}Ga_{0.95}N$ quantum wells (instead of GaN) allowed us to achieve better strain compensation of $Al_{0.966}In_{0.04}N/In_{0.05}Ga_{0.95}N$ superlattices to GaN substrate. Structures with $20x$ QWs (with well width in the range 1.1 nm–3 nm and barriers width of 3 nm) grown on GaN/sapphire templates and bulk GaN crystals are crack free, as demonstrated by Nomarski contrast and scanning electron microscopic measurements. The performed XRD mapping of 'a' and 'c' constants show that AlInN/InGaN MQWs are fully strained — *i.e.* lattice constant 'a' of MQWs is equal to lattice constant 'a' of GaN substrate. We demonstrated IS absorption at room temperatures on these structures in the range 2.45 μm–1.52 μm (see Figs. 29 and 30) [94]. The AlInN/InGaN strain compensated MQW structures grown by PA-MBE on GaN substrates, thanks to the crackless growth and good optical quality, are very attractive for telecommunication applications at 1.5 μm wavelengths like electro-optical modulators or all optical switches. Due to the low value of the refractive index, AlInN/InGaN superlattices can also replace AlGaN/GaN in thick cladding layers in nitride optoelectronic devices *e.g.* in blue-violet laser diodes.

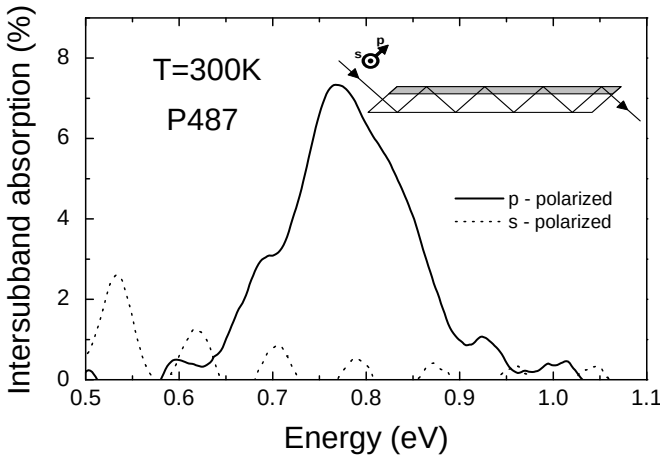


Fig. 29. The intersubband absorption measurements performed at room temperature in the multipass waveguide configuration (see insert). Results for *p*-polarization and *s*-polarization are shown as a continuous and dotted lines respectively.

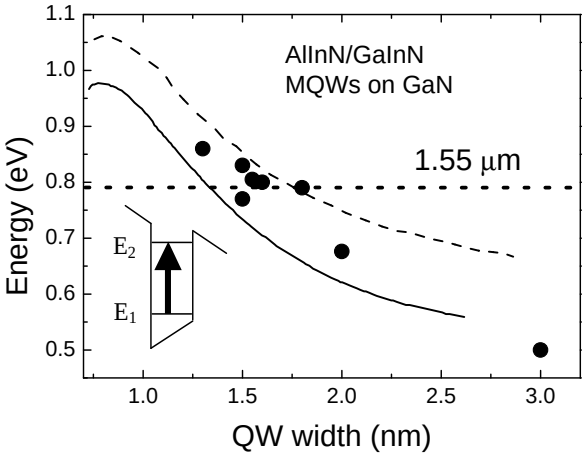


Fig. 30. Energy of E_{12} transition between first E_1 and second E_2 electronic levels in QWs as a function of the QWs width. Experimental data for AlInN/GaInN MQWs structures shown as dots. The lines show calculation results, which has been for AlN/GaN MQWs (with 3 nm thick AlN barriers). The solid and dashed lines correspond to undoped quantum wells and doped with Si at a level of 5×10^{19} cm^{-3}, respectively.

We show that making use of Ga and In surfactants, the high quality nitride devices can be grown by PA-MBE at relatively low growth temperatures. Growth of efficient InGaN QWs together with high p-type doping levels in InGaN:Mg allowed us to demonstrate first blue-violet laser diodes. With continuing improvements in the quality of bulk GaN substrates and further optimization of the PA-MBE growth conditions the technique is well positioned to become a viable alternative to the MOCVD technology in a field of high power UV and green LDs in the near future.

4. Conclusions

The results presented in this review summarize long time research program based on application of various physical methods in the physics and technology of group III metal nitride semiconductors. The most essential results, obtained in the Institute of High Pressure Physics, can be listed as follows:

— the thermodynamic properties of group III metal systems in pressures up to 20 kbar and temperature up to 2000 K have been determined;

— the kinetic properties of the adsorption and dissolution reaction of molecular nitrogen in liquid group III metals have been described;

— crystal growth of substrate quality GaN crystals has been investigated. The research led to the development of the technology of the growth of substrate quality n-type GaN crystals for optoelectronics;

— the two basic epitaxy methods: MOVPE and MBE, were developed and applied for deposition of high quality homoepitaxial layers and quantum well structures;

— the development of dislocation free nitride layers and structures allows to extend the temperature range used in epitaxy for blue power LDs. This opens the possibility of construction of high power green and UV LDs;

— the development of the QW structures and processing technology allowed to obtain blue LDs of the efficiency comparable with the best heteroepitaxial devices.

The research presented in this paper has been supported by the Polish State Committee for Scientific Research grants 8 T11 G 001 2000 C/5013 and 7 T08A 015 18 and in part by European Commission within the: Support for Centers of Excellence No ICA1-CT-2000-70005. We would like to acknowledge the financial support from EU within GaNano project STREP 505641-1. The calculations presented here used computing facilities of Interdisciplinary Centre for Mathematical and Computational Modeling of Warsaw University (ICM UW).

REFERENCES

[1] S. Nakamura, G. Fasol, *The Blue Laser Diodes*, Springer Verlag, Berlin 1997.

[2] J.V. Lirman, H.S. Zhdanov, *Acta Physicochem. USSR* **6**, 306 (1930).

[3] W. Utsumi, H. Saitoh, H. Kaneko, T. Watanuki, K. Aoki, O. Shimomura, *Nature Materials* **2**, 735 (2003).

[4] S. Porowski, I. Grzegory, *J. Cryst. Growth* **178**, 174 (1997).

[5] I. Grzegory, S. Krukowski, M. Leszczynski, P. Perlin, T. Suski, S. Porowski, *Acta Phys. Pol. A Suppl.* **100**, 57 (2001).

[6] K. Motoki, T. Okahisa, S. Nakahata, N. Matsumoto, H. Kimura, H. Kasai, K. Takemoto, K. Uematsu, M. Ueno, Y. Kumagai, A. Koukitu, H. Seki, *Mater. Sci. Eng.* **B93**, 123 (2002).

[7] Y. Oshima, T. Eri, M. Shibata, H. Sunakawa, A. Usui, *Phys. Stat. Solidi* **C1**, 554 (2002).

[8] E. Richter, Ch. Hennig, M. Weyers, F. Habel, J.D. Tsay, W.Y. Liu, P. Bruckner, F. Scholz, Yu. Makarov, A. Segal, J. Kaeppeler, *J. Cryst. Growth* **277**, 6 (2005).

[9] K. Motoki, T. Okahisa, S. Nakahata, N. Matsumoto, H. Kimura, H. Kasai, K. Takemoto, K. Uematsu, M. Ueno, Y. Kumagai, A. Koukitu, H. Seki, *J. Cryst. Growth* **237-239**, 912 (2002).

[10] H.P. Maruska, J.J. Tjetjen, *Appl. Phys. Lett.* **15**, 327 (1969).

[11] J.I. Pankove, H.P. Maruska, J.E. Berkeyheiser. *Appl. Phys. Lett.* **17**, 197 (1970).

[12] J.I. Pankove, E.A. Miller, D. Richman, J.E. Berkeyheiser *J. Lum.* **4**, 63 (1971).

[13] E.K. Sichel, J.I. Pankove *J. Phys. Chem. Solids* **38**, 330 (1977).

[14] H. Amano, M. Kito, K. Hiramatsu, I. Akasaki, *Jpn. J. Appl. Phys. Part. 2-Letters* **28**, L2112 (1989).

[15] S. Nakamura, T. Mukai, M. Senoh, N. Iwasa, *Jpn. J. Appl. Phys. Part. 2-Letters* **31**, L139 (1992).

[16] S. Nakamura, IEICE Trans. E83-C, (2000) 529.

[17] Strategies Unlimited Gallium Nitride — 2000: Technology Status, Applications, and Market Forecasts, May 31 2000, Mountain View, CA, USA.

[18] C. Wetzel, T. Detchprohm, *MRS Int. J. Nitride Semicond. Res.* **10**, 2 (2005).

[19] G.A. Slack, T.F. McNelly, *J. Cryst. Growth* **34**, 263 (1976).

[20] J.A. Van Vechten, *Phys. Rev.* **B7**, 1479 (1973).

[21] J. Karpinski, J. Jun, S. Porowski, *J. Cryst. Growth* **66**, 1 (1984).

[22] J. Karpinski, S. Porowski, *J. Cryst. Growth* **66**, 11 (1984).

[23] F.P. Bundy, *Physica A* **156**, 169 (1989).

[24] T. Massalski (ed) *Binary Alloy Phase Diagrams ASM International*, vol. 1, 1992.

[25] I. Grzegory, S. Krukowski, J. Jun, M. Bockowski, M. Wroblewski, S. Porowski, *AIP Conf. Proc.* **309**, 565 (1994).

[26] S. Krukowski, A. Witek, J. Adamczyk, J. Jun, M. Bockowski, I. Grzegory, B. Lucznik, G. Nowak, M. Wroblewski, A. Presz, S. Gierlotka, S. Stelmach, B. Palosz, S. Porowski, P. Zinn, *J. Phys. Chem. Solids* **59**, 289 (1998).

[27] E. Monberg, in *Handbook of Crystal Growth 2. Bulk Crystal Growth A. Basic Techniques*, ed. D.T.J. Hurle, North-Holland, Amsterdam 1994, p. 51

[28] D.T.J. Hurle, B. Cockayne, in *Handbook of Crystal Growth 2. Bulk Crystal Growth A. Basic Techniques*, ed. D.T.J. Hurle, North-Holland, Amsterdam 1994, p. 99.

[29] I. Grzegory, PhD Thesis, Warsaw 1995 (in Polish).

[30] W.P. Glushko (ed.) Termodinamiczeskije Swojstwa Indiwidualnych Weszczestw, Nauka, Moscow 1979 (in Russian).

[31] W.E. Zinowiev, *Teplofiziczeskije Swojstwa Metallow pri Wysokich Temperaturach*, Moscow Metallurgia 1989 (in Russian).

[32] B. Delley, *J. Chem. Phys.* **92**, 508 (1990).

[33] Z. Romanowski, S. Krukowski, I. Grzegory, S. Porowski, *J. Chem. Phys.* **114**, 6353 (1990).

[34] Z. Romanowski, S. Krukowski, I. Grzegory, S. Porowski, *J. Cryst. Growth* **189/190**, 159 (1998).

[35] S. Porowski, M. Bockowski, B. Łucznik, M. Wroblewski, S. Krukowski, I. Grzegory, M. Leszczyński, G. Nowak, K. Pakula, J.M. Baronowski, *III-V Nitrides Symposium. Mater. Res. Soc.*, 1997 p. 35.

[36] S. Krukowski, I. Grzegory, M. Bockowski, B. Łucznik, T. Suski, G. Nowak, J. Borysiuk, M. Wroblewski, M. Leszczynski, P. Perlin, S. Porowski, J.L. Weyher, *Int. J. Mater. Product Techn.* **22**, 226 (2005).

[37] I. Grzegory, M. Boćkowski, B. Łucznik, S. Krukowski, Z. Romanowski, M. Wróblewski, S. Porowski, *J. Cryst. Growth* **246**, 177 (2002).

[38] Z. Liliental-Weber, *EMIS Datareview Series No23*, published by INSPEC, The Institution of Electrical Engineers, London 1999, p. 230.

[39] J.L. Rouviere, J.L. Weyher, M. Seelmann-Eggebert, S. Porowski, *Appl. Phys. Lett.* **73**, 668 (1998).

[40] M. Seelmann-Eggebert, J.L. Weyher, H. Obloh, H. Zimmermann, A. Rar, S. Porowski, *J. Cryst. Growth* **210**, 151 (2000).

[41] J.D. Gunton, M. Droz, *Introduction to the Theory of Metastable and Unstable States*, Springer, Berlin 1983.

[42] S. Krukowski, M. Bockowski, B. Lucznik, I. Grzegory, S. Porowski, T. Suski, Z. Romanowski, *J. Phys. Condens. Matter* **13**, 8881 (2001).

[43] P. Perlin, J. Camassel, W. Knap, T. Talercio, J.C. Chervin, T. Suski, I. Grzegory, S. Porowski, *Appl. Phys. Lett.* **67**, 2524 (1995).

[44] E. Litwin-Staszewska, T. Suski, R. Piotrzkowski, I. Grzegory, M. Boćkowski, J.L. Robert, L. Konczewicz, D. Wasik, E. Kaminska, D. Cote, B. Clerjaud, *J. Appl. Phys.* **89**, 7960 (2001).

[45] K. Saarinen, T. Laine, S. Kuisma, P. Hautojarvi, L. Dobrzyński, J.M. Baranowski, K. Pakuła, R. Stępniewski, M. Wojdak, A. Wysmołek, T. Suski, M. Leszczyński, I. Grzegory, S. Porowski, *Phys. Rev. Lett.* **79**, 3030 (1997).

[46] J. Neugebauer, C.G. Van de Walle, *Phys. Rev.* **B50**, 8067 (1994).

[47] P. Boguslawski, E.L. Briggs, J. Bernholc, *Phys. Rev.* **B51**, 17255 (1995).

[48] S. Porowski, M. Boćkowski, B. Łucznik, I. Grzegory, M. Wróblewski, H. Teisseyre, M. Leszczynski, E. Litwin-Staszewska, T. Suski, P. Trautman, K. Pakuła, J.M. Baranowski, *Acta Phys. Pol. A*, **92**, 958 (1997).

[49] E. Frayssinet, W. Knap, S. Krukowski, P. Perlin, P. Wisniewski, T. Suski, I. Grzegory, S. Porowski, *J. Cryst. Growth* **230**, 442 (2001).

[50] T. Suski, J. Jun, M. Leszczynski, H. Teisseyre, I. Grzegory, S. Porowski, G. Dollinger, K. Saarinen, T. Laine, J. Nissila, W. Burkhard, W. Kriegseis, B.K. Meyer, *Mat. Sci. Eng.* **B59**, 1 (1998).

[51] M. Leszczynski, I. Grzegory, H. Teisseyre, T. Suski, M. Bockowski, J. Jun, J.M. Baranowski, S. Porowski, J. Domagala, *J. Cryst. Growth* **169**, 235 (1996).

[52] S.H. Christiansen, M. Albrecht, H.P. Strunk, C.T. Foxon, D. Korakakis, I. Grzegory, S. Porowski, *Phys. Stat. Solidi (a)* **176**, 285 (1999).

[53] Z. Liliental-Weber, M. Benamara, W. Swider, J. Washburn, I. Grzegory, S. Porowski, R.D. Dupuis, C.J. Eiting, *Physica B* **273-274**, 124 (1999).

[54] J.L. Weyher, P.D. Brown, J.L. Rouviere, T. Wosinski, A.R.A. Zauner, I. Grzegory, *J. Cryst. Growth* **210**, 151 (2000).

[55] J.L. Weyher, S. Müller, I. Grzegory, S. Porowski, *J. Cryst. Growth* **182**, 17 (1997).

[56] P. Prystawko, R. Czernecki, M. Leszczynski, P. Perlin, P. Wisniewski, L. Dmowski, H. Teisseyre, T. Suski, I. Grzegory, M. Bockowski, G. Nowak, S. Porowski, *Phys. Stat. Solidi (b)* **216**, 320 (1999).

[57] S. Krukowski, M. Bockowski, I. Grzegory, B. Lucznik, G. Nowak, M. Wroblewski, M. Leszczynski, G. Teisseyre, T. Suski, S. Porowski, Proceedings-of-the-Second-Symposium-on-III-V-Nitride-Materials-and-Processes. Electrochem. Soc, Pennington, NJ, USA 1998, 189-200.

[58] M. Conway, J. S. Willams, C. Jagadish, private communication.

[59] P. Prystawko, M. Leszczynski, B. Beaumont, P. Gibart, E. Frayssinet, W. Knap, P. Wisniewski, M. Bockowski, T. Suski, S. Porowski, *Phys. Stat. Solidi (b)* **210**, 437 (1998).

[60] M. Leszczynski, B. Beaumont, E. Frayssinet, W. Knap, P. Prystawko, T. Suski, I. Grzegory, S. Porowski, *Appl. Phys. Lett.* **75**, 222 (1999).

[61] M. Leszczynski, H. Teisseyre. T. Suski, I. Grzegory, M. Bockowski, J. Jun, S. Porowski, K. Pakula, J.M. Baranowski, C.T. Foxon, T.S. Cheng, *Appl. Phys. Lett.* **69**, 73 (1996).

[62] A. Wysmolek, M. Potemski, R. Stepniewski, J. Lusakowski, K. Pakula, J.M. Baranowski, G. Martinez, P. Wyder, I. Grzegory, S. Porowski, *Phys. Stat. Sol. (b)* **216**, 11 (1999).

[63] C. Kirchner, V. Schwegler, F. Eberhard, M. Kamp, K.J. Ebeling, K. Kornitzer, T. Ebner, K. Thonke, R. Sauer, P. Prystawko, M. Leszczynski, I. Grzegory, S. Porowski, *Appl. Phys. Lett.* **75**, 1098 (1999).

[64] M. Leszczynski, P. Prystawko, R. Czernecki, J. Lehnert, T. Suski, P. Perlin, P. Wisniewski, I. Grzegory, G. Nowak, S. Porowski, M. Albrecht, *J. Cryst. Growth* **231**, 352 (2001).

[65] G. Kamler, J. Weyher, I. Grzegory, E. Jezierska, T. Wosinski, *J. Cryst. Growth* **246**, 21 (2002).

[66] P. Wiśniewski, R. Czernecki, P. Prystawko, M. Maszkowicz, M. Leszczyński, T. Suski, I. Grzegory, S. Porowski, M. Marona, T. Świetlik, P. Perlin, to be published in Proceedings of SPIE — Photonics West Conference, San Jose, January 2006.

[67] P. Perlin, Wiśniewski, R. Czernecki, P. Prystawko, M. Leszczyński, T. Suski, I. Grzegory, L. Marona, T. Świetlik, K. Komorowska, S. Porowski, to be published in Proceedings of SPIE — Photonics Europe Conference, Strasbourg, March 2006.

[68] L. Hildebrandt, R. Knispel, S. Stry, J.R. Sacher, F. Schael, *Appl. Optics* **42**, 2110 (2003).

[69] H. Morkoc, *J. Mater. Sci.: Materials in Electronics* **12**, 677 (2001).

[70] T.D. Moustakas, E. Iliopoulos, A.V. Sampath, H.M. Ng, D. Doppalapudi, M. Misra, D. Korakakis, R. Singh, *J. Cryst. Growth* **227-228**, 13 (2001).

[71] M. Kauer, S. E. Hooper, V. Bousquet, K. Johnson, C. Zellweger, J.M. Barnes, J. Windle, T.M. Smeeton, J. Heffernan, *Electron. Lett.* **41**, 739 (2004).

[72] N. Grandjean, B. Damilano, J. Massies, *J. Phys.: Condens. Matter* **13**, 6945 (2001).

[73] M.J. Manfra, K.W. Baldwin, M. Sergent, R.J. Molnar, J. Caissie, *Appl. Phys. Lett.* **85**, 1722 (2004).

[74] P. Waltereit, H. Sato, C. Poblenz, D.S. Green, J.S. Brown, M. McLaurin, T. Katona, S.P. DenBaars, J.S. Speck, J.-H. Liang, M. Kato, H. Tamura, S. Omori, C. Funaoka, *Appl. Phys. Lett.* **84**, 2748 (2004).

[75] C.T. Foxon, T.S. Cheng, S.V. Novikov, D. Korakakis, N.J. Jeffs, I. Grzegory, S. Porowski, *J. Cryst. Growth* **207**, 1 (1999).

[76] B. Heying, I. Smorchkova, C. Poblenz, C. Elsass, P. Fini, S. Den Baars, U. Mishra, J.S. Speck, *Appl. Phys. Lett.* **77**, 2885 (2000).

[77] C. Adelmann, J. Brault, D. Jalabert, P. Gentile, H. Mariette, G. Mula, B. Daudin, *J. Appl. Phys.* **91**, 9638 (2002).

[78] C. Skierbiszewski, Z. Wasilewski, M. Siekacz, A. Feduniewicz, B. Pastuszka, I. Grzegory, M Leszczynski, S. Porowski, *Phys. Stat. Solidi (a)* **201**, 320 (2004).

[79] C. Skierbiszewski, K. Dybko, W. Knap, J. Łusakowski, M. Siekacz, W. Krupczyński, G. Nowak, M. Boćkowski, Z. Wasilewski, D. Maude, T. Suski, S. Porowski, *Appl. Phys. Lett.* **86**, 102106 (2005).

[80] C. Skierbiszewski, Z. Wasilewski, M. Siekacz, A. Feduniewicz, P. Perlin, P. Wisniewski, J. Borysiuk, I. Grzegory, M. Leszczynski, T. Suski, S. Porowski, *Appl. Phys. Lett.* **86**, 011114 (2005).

[81] J. Neugebauer, T.K. Zywietz, M. Scheffler, J.E. Northrup, H. Chen, R.M. Feenstra, *Phys. Rev. Lett.* **70**, 56101 (2003).

[82] J.E. Northrup, J. Neugebauer, R.M. Feenstra, A.R. Smith, *Phys. Rev.* **B61**, 9932 (2000).

[83] T. Zywietz, J. Neugebauer, M. Scheffler, *Appl. Phys. Lett.* **73**, 487 (1998).

[84] I.P. Smorchkova, E. Haus, B. Heying, P. Kozodoy, P. Fini, J.P. Ibbetson, S. Keller, S.P. DenBaars, J.S. Speck, U.K. Mishra, *Appl. Phys. Lett.* **76**, 718 (2000).

[85] E. Haus, I.P. Smorchkova, B. Heying, P. Fini, C. Poblenz, T. Mates, U.K. Mishra, J.S. Speck, *J. Cryst. Growth* **246**, 55 (2002).

[86] A.J. Ptak, T.H. Myers, L.T. Romano, C.G. Van de Walle, J.E. Northrup, *Appl. Phys. Lett.* **78**, 285 (2001).

[87] V. Ramachandran, R.M. Feenstra, W.L. Sarney, L. Salamanca-Riba, J.E. Northrup, L.T. Romano, D.W. Greve, *Appl. Phys. Lett.* **75**, 808 (1999).

[88] L.T. Romano, J.E. Northrup, A.J Ptak, T.H. Myers, *Appl. Phys. Lett.* **77**, 2479 (2000).

[89] J.E. Nortrup, *Appl. Phys. Lett.* **82**, 2278 (2003).

[90] A. Feduniewicz, C. Skierbiszewski, M. Siekacz, Z. Wasilewski, I. Sproule, S. Grzanka, J. Borysiuk, G. Kamler, E. Litwin-Staszewska, R. Czernecki, M. Boćkowski, S. Porowski, *J. Cryst. Growth* **278**, 443 (2005).

[91] J. Faist, F. Capasso, D.L. Sivco, C. Sirtori, A.L. Hutchinson, A.Y. Cho, *Science* **264**, 553 (1994).

[92] B.F. Levine, K.K. Choi, C.G. Bethea, J. Walker, R.J. Malik, *Appl. Phys. Lett.* **50**, 1092 (1987).

[93] J.-F. Carlin, M. Ilegems, *Appl. Phys. Lett.* **83**, 668 (2003).

[94] C. Skierbiszewski, G. Cywiński, M. Siekacz, A. Feduniewicz-Zmuda, L. Nevou, L. Doyennette, M. Tchernycheva, F. H. Julien, J. Smalc, P. Prystawko, M. Kryśko, S. Grzanka, I. Grzegory, J.Z. Domagała, T. Remmele, M. Albrecht, S. Porowski, in *Gallium Nitride Materials and Devices*, eds C.W. Litton, J.G. Grote, H. Morkoc, A. Madhukar, *Proc. of SPIE* **6121**, 2006, p. 612109.